nature communications

Article

https://doi.org/10.1038/s41467-025-62956-8

Cholecystectomy-related gut microbiota dysbiosis exacerbates colorectal tumorigenesis

Received: 9 September 2023

Accepted: 31 July 2025

Published online: 16 August 2025

Check for updates

Bo Tang[1,5], Shengpeng Li[1,5], Xin Li[1,5], Jialin He[1], An Zhou[1], Lingyi Wu[1], Xu Xiao[1], Sumin Wang[1], Hongfei Jiang[1], Jincheng Jian[1], Zhanjie Hou[1], Yusong Ge[1], Yuanyuan Lei[1], Jianchun Zhou[1], Dianji Tu[1,2], Cheng Lu[1] ✉, Min Yang[1] ✉ & Shiming Yang[1,3,4] ✉

Cholecystectomy represents the most prevalent biliary surgical procedure for gallbladder abnormalities. Growing evidence suggests that cholecystectomy is associated with an elevated risk of colorectal cancer. However, the underlying mechanism remains elusive. Here we show that cholecystectomy exacerbates colorectal tumorigenesis in both AOM/DSS and $APC^{min/+}$ mice models. Metagenomic sequencing and targeted metabolomics show that cholecystectomy leads to a decrease of *Bifidobacterium breve (B. breve)* and an increase of *Ruminococcus gnavus (R. gnavus)*, along with increased levels of glycoursodeoxycholic acid (GUDCA) in human and tauroursodeoxycholic acid (TUDCA) in mice. Fecal microbiota transplantation, single bacterial colonization and bile acid supplementation demonstrate that cholecystectomy-related gut microbiota perturbations promote the production of TUDCA and facilitate colorectal tumorigenesis. RNA-sequencing and co-immunoprecipitation reveal that the compromised bile acid metabolism inhibits farnesoid X receptor (FXR) signaling, disrupts the FXR/β-catenin interaction, and ultimately exacerbates colorectal tumorigenesis. Significantly, FXR agonist obeticholic acid (OCA) averts cholecystectomy-related colorectal tumorigenesis. The gut microbiota holds a crucial position in cholecystectomy-induced colorectal tumorigenesis, and modulation of the gut microbiota-bile acid-FXR axis represents a promising preventive strategy.

In the wake of alterations in dietary structure, the prevalence of gallbladder disorders such as gallstones and gallbladder polyps has shown a gradual increase on a global scale[1]. Cholecystectomy, which represents the most frequently performed biliary surgical intervention, is regarded as the standard therapeutic approach for patients afflicted with gallbladder ailments. Cholecystectomy was formerly perceived as virtually harmless. Nevertheless, accumulating evidence suggests that there is a notable increase in the incidence of post-cholecystectomy syndromes[2] and diseases related to metabolic syndrome[3,4]. Importantly, previous clinical investigations demonstrated that cholecystectomy is associated with an elevated risk of colorectal cancer[5–7], while the underlying mechanism remains unidentified.

The gallbladder is responsible for storing and concentrating bile. Cholecystectomy gives rise to a diminished bile acid pool and an

[1]Department of Gastroenterology, Xinqiao Hospital, Army Medical University, Chongqing, China. [2]Laboratory Medicine Center, Xinqiao Hospital, Army Medical University, Chongqing, China. [3]Chongqing Institute for Brain and Intelligence, Guangyang Bay Laboratory, Chongqing, China. [4]Chongqing Municipality Clinical Research Center for Gastroenterology, Chongqing, China. [5]These authors contributed equally: Bo Tang, Shengpeng Li, Xin Li.
✉e-mail: lucheng1108@tmmu.edu.cn; Yangmin1990@tmmu.edu.cn; Yangshiming@tmmu.edu.cn

increased rate of enterohepatic recirculation of bile acids, thereby inducing a conspicuous increase in the entry of bile acids into the intestine and their interaction with the gut microbiome[8]. The interplay between bile acids and the gut microbiota is bidirectional. The intestinal flora participates in the metabolism of bile acids and affects the composition of bile acids[9]. Alterations in bile acid profiles can further reshape the gut microbiota by facilitating the growth of bile acid metabolizing bacteria and inhibiting the growth of bile-sensitive bacteria[10].

FXR, a nuclear receptor for bile acids, is highly expressed in both liver and intestine[9]. The intestinal microbiota might regulate FXR signaling by modulating bile acid metabolism[11]. Intriguingly, bile acids could affect the intestinal bacteria by regulating FXR. Previous studies have revealed that FXR expression is inhibited during the transition from colorectal adenoma to tumor[9]. Notably, studies have reported that antagonism of intestinal FXR induces proliferation and DNA damage in $Lgr5^+$ cells[12]. However, the underlying mechanism of gut microbiota-FXR signaling in cholecystectomy-induced colorectal tumorigenesis is still unclear.

In this work, we demonstrate that cholecystectomy induces significant alterations in the gut microbiota and bile acid profiles, and these changes exacerbate colorectal tumorigenesis. Here, we aim to explore the specific role of the gut microbiota in cholecystectomy-associated colorectal tumorigenesis and elucidate the underlying mechanisms.

Results

Cholecystectomy exacerbates colorectal tumorigenesis in both AOM/DSS and $APC^{min/+}$ mice

We initially explored the role of cholecystectomy alone on body weight, the gut barrier, and intestinal barrier function. The results showed that there was no significant change in body weight (Supplementary Fig. 1a) and H&E staining (Supplementary Fig. 1b) in the cholecystectomy (GBx) group compared with the Sham group. The intestinal barrier function of GBx mice was slightly impaired without significant difference (Supplementary Fig. 1c). Nevertheless, expression of the barrier-related molecules ZO-1(Supplementary Fig. 1d) and Occludin (Supplementary Fig. 1e) was significantly lower subsequent to GBx. To further evaluate the impact of cholecystectomy on colorectal tumorigenesis, we conducted cholecystectomy prior to AOM/DSS treatment in C57BL/6 J mice (Fig. 1a). The average body weight was lower in GBx+AOM/DSS mice (Fig. 1b). Mouse colonoscopy revealed the presence of macroscopic tumors in GBx+AOM/DSS mice (Fig. 1c). Importantly, the average number and distribution of tumors were increased in GBx+AOM/DSS mice (Fig. 1d, e). Histological examination confirmed that GBx+AOM/DSS mice developed a higher proportion of adenocarcinoma and high-grade dysplasia (Fig. 1f). GBx+AOM/DSS mice displayed impaired intestinal barrier function and exhibited a greater number of Ki-67-positive cells (Fig. 1g, h). In addition, cholecystectomy led to an increase in the serum levels of the biomarker CEA and CA19-9 (Fig. 1i).

We further established a GBx model in transgenic $APC^{min/+}$ mice (Supplementary Fig. 2a). The body weight of APC-GBx mice displayed a decreasing tendency, although the difference was not significant (Supplementary Fig. 2b). There was no significant difference in the total tumor number between the two groups (Supplementary Fig. 2c, d). The proportion of polyps with a diameter exceeding 2 mm was significantly elevated in APC-GBx mice (Supplementary Fig. 2d). Moreover, histological examination confirmed that APC-GBx mice exhibited a higher proportion of adenocarcinoma and high-grade dysplasia (Supplementary Fig. 2e), along with a greater number of Ki-67-positive cells (Supplementary Fig. 2f). The intestinal barrier function of APC-GBx mice was slightly impaired (Supplementary Fig. 2g). The level of CEA in APC-GBx mice was significantly higher, while there was no significant difference in the level of CA19-9 (Supplementary Fig. 2h, i). We also examined the occurrence of intestinal polyps in $APC^{min/+}$ mice after cholecystectomy. As shown in Supplementary Fig. 2j, the number of polyps in the small intestine was not significantly changed. However, APC-GBx mice tended to develop large (> 2 mm) adenomas (Supplementary Fig. 2k). Histopathologic analysis showed that APC-GBx mice had a higher proportion of low-grade adenoma, high-grade adenoma and adenocarcinoma (Supplementary Fig. 2l). Collectively, these findings suggest that cholecystectomy exacerbates colorectal tumorigenesis in both AOM/DSS and $APC^{min/+}$ mice.

Cholecystectomy exacerbates colitis in the AOM/DSS model

To further explore the relationship between cholecystectomy and carcinogenesis, a dynamic histological examination of colon sections was conducted. The results showed that colorectal tumorigenesis in GBx+AOM/DSS group occurred at a significantly earlier stage (Supplementary Fig. 3). To determine the effect of GBx on the progression of colitis in mice, the level of inflammation during the early and late stages within the model was examined. DAI score was increased in the GBx+AOM/DSS group, both in weeks 4 and 10 following AOM injection (Fig. 2a). The lengths of colons were notably shorter at both these time points (Fig. 2b). Moreover, histological analysis revealed an increase in inflammation and the extent of lesions at week 4 (Fig. 2c). Typical characteristics of chronic colitis, encompassing epithelial cell damage and inflammatory cell infiltration, were induced at week 10 (Fig. 2c) in the GBx+AOM/DSS mice. The expression of ZO-1 (Fig. 2d) and Occludin (Fig. 2e) was lower in GBx+AOM/DSS mice at both time points. Furthermore, the expression of IL-1β (Fig. 2f) and TNF-α (Fig. 2g) was significantly increased both in weeks 4 and 10. Our data suggest that cholecystectomy could exacerbate early and late colitis in the AOM/DSS model.

Cholecystectomy-related gut microbiota dysbiosis is implicated in colorectal tumorigenesis

To validate the impact of the cholecystectomy-related gut microbiota on colorectal tumorigenesis, mice were gavaged with antibiotic cocktails before AOM/DSS administration (Supplementary Fig. 4a). ABX-Sham mice and ABX-GBx mice showed indistinguishable colorectal tumor numbers (Supplementary Fig. 4b, c), histological examination (Supplementary Fig. 4d), intestinal permeability (Supplementary Fig. 4e), and serum oncological indicators (Supplementary Fig. 4f, g). Subsequently, fecal microbiota transplantation (FMT) experiments were conducted using feces from healthy control (FMT-HC) and cholecystectomy patients (FMT-GBx), respectively (Fig. 3a). The colorectal tumor number was significantly increased in FMT-GBx group (Fig. 3b and Supplementary Fig. 5a). Histological examination confirmed that FMT-GBx mice developed a higher proportion of high-grade dysplasia and adenocarcinoma (Fig. 3c). Moreover, FMT-GBx mice exhibited significantly higher levels of intestinal permeability, CEA and CA19-9 (Supplementary Fig. 5b–d) compared to the FMT-HC mice. Consistently, we performed FMT experiments using feces from Sham +AOM/DSS (FMT-Sham) and GBx+AOM/DSS mice (FMT-GBx), respectively (Fig. 3d). Consistently, FMT-GBx mice had an increased number of tumors (Fig. 3e and Supplementary Fig. 6a), a higher proportion of advanced pathological features (Fig. 3f), and higher levels of intestinal permeability, CEA and CA19-9 (Supplementary Fig. 6b–d). A cohousing experiment was further conducted to validate the role of the gut microbiota in colorectal tumorigenesis. Mo-housed GBx mice exhibited a progressive feature of colorectal tumorigenesis (Fig. 3g, h and Supplementary Fig. 7a) and increased levels of intestinal permeability (Supplementary Fig. 7b) and tumor serological indices (Supplementary Fig. 7c, d). In contrast, cohoused GBx and cohoused sham mice displayed similar features (Fig. 3g, h and Supplementary Fig. 7a–d). Taken together, these results demonstrated that cholecystectomy promoted colorectal tumorigenesis in a gut microbiota-dependent manner.

https://doi.org/10.1038/s41467-025-62956-8

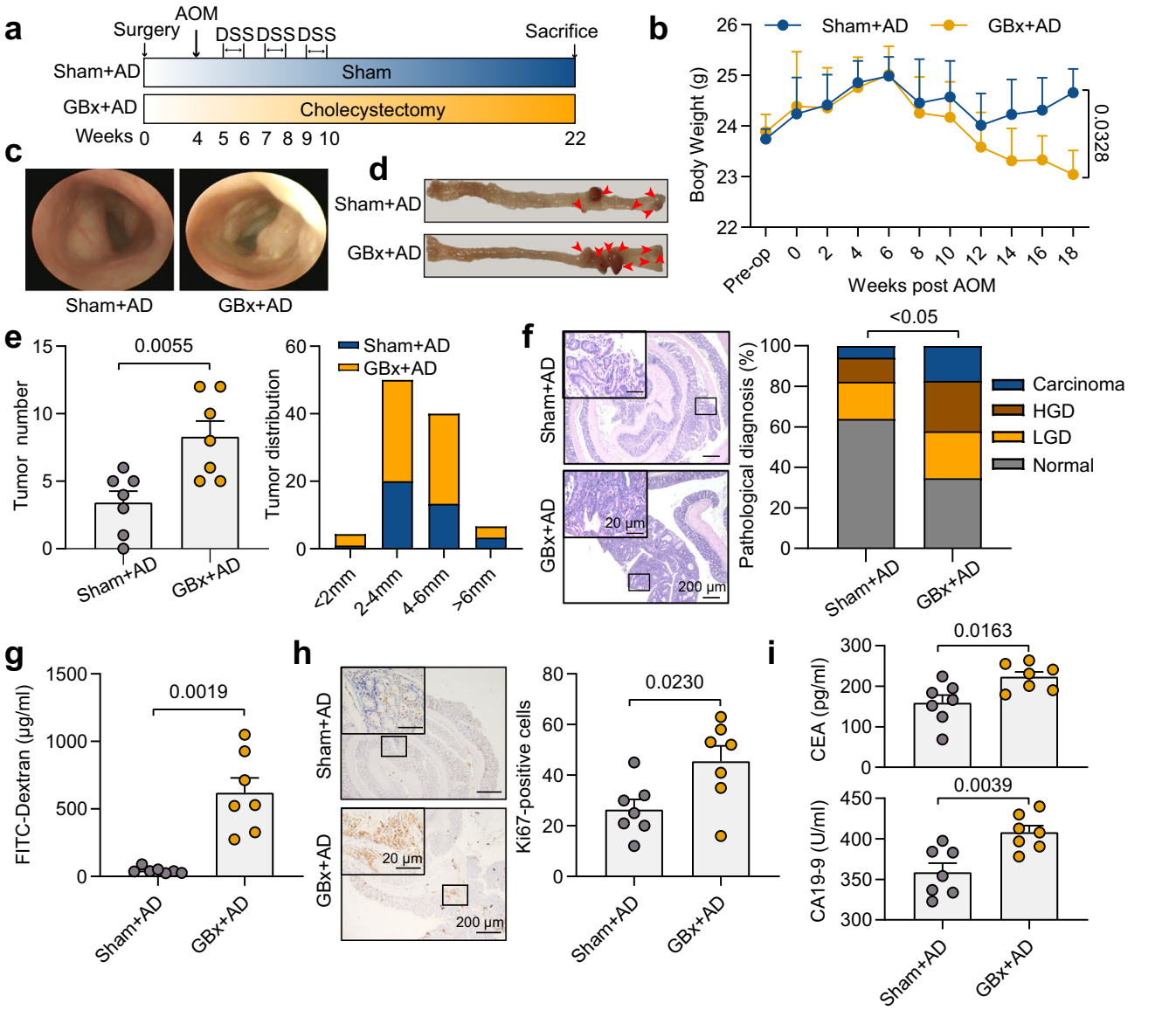

Fig. 1 | Cholecystectomy exacerbates colorectal tumorigenesis in C57BL/6 mice. a Schematic diagram showing the experimental design and timeline. **b** The body weight of mice (two-tailed *t* test was used at the end point, $n = 7$/group). **c** Representative colonoscopy images of mice ($n = 3$/group). Macroscopic tumors were present in GBx+AD mice but no obvious tumor was observed in Sham+AD mice. **d** Colonic morphologies. Each red arrow points at one tumor location ($n = 7$/group). **e** Tumor number (left) ($n = 7$/group) and tumor size distribution (right). **f** Representative H&E staining of mouse colons (left). H&E staining showed normal, dysplastic mucosae and carcinoma in the colon tissues. The pathological score was quantitative analyzed (right) according to the following criteria: 0 for normal; 1 for LGD; 2 for HGD and 3 for carcinoma (ANOVA, $n = 7$/group). The bottom scale bar is 200 μm and the top scale bar is 20 μm. **g** Intestinal permeability was measured by FITC-dextran (two-tailed Welch's *t* test, $n = 7$/group). **h** Representative images and semiquantitative analysis of Ki67 staining of mouse colons ($n = 7$/group). **i** Serum CEA (upper) and CA19-9 (lower) levels in the two groups ($n = 7$/group). Data are shown as the mean ± SEM. *P* values were determined by two-tailed *t* test for **e, h, i** and were indicated in each figure. GBx, cholecystectomy; AOM, azoxymethane; DSS, dextran sodium sulfate; AD, AOM/DSS; CEA, carcinoembryonic antigen; CA19-9, cancer antigen 19-9; LGD: low grade dysplasia; HGD: high grade dysplasia. Source data are provided as a Source Data file.

To deeply explore the changes in specific gut microbiota after cholecystectomy and their roles in CRC oncogenesis, we subsequently collected fecal and serum samples from 52 patients who underwent cholecystectomy and 45 healthy controls. The demographic characteristics and clinical indicators are listed in Supplementary Table 1. Notably, two patients developed CRC after cholecystectomy. Specifically, one case occurred four years after cholecystectomy, and the other occurred six years after cholecystectomy. Besides, there were no significant differences in liver function indicators and liver diseases that occurred during the follow-up process between the two groups. The α-diversity decreased significantly at both the genus and species levels after cholecystectomy (Fig. 4a). There was a significant difference between the two types of microbiomes (Fig. 4b). *Bifidobacterium breve* (*B. breve*) was the top microbial species contributing to group separation (Fig. 4c). To examine the impact of cholecystectomy alone on the gut microbiota, shotgun metagenomic sequencing was carried out on fecal samples from sham and GBx mice. The diversity of gut microbiota was not significantly changed between both groups (Supplementary Fig. 8a, b). Subsequently, the microbiota in mice subsequent to AOM/DSS treatment was examined. The diversity of gut microbiota exhibited a change between the Sham+AOM/DSS and GBx +AOM/DSS groups (Fig. 4d, e). *Ruminococcus gnavus (R. gnavus)* was the most significant species contributing to group separation (Fig. 4f). We further verified the abundance of these two bacteria in both the human cohort and the GBx+AOM/DSS model. We observed that the abundance of *B. breve* significantly decreased, while *R. gnavus*

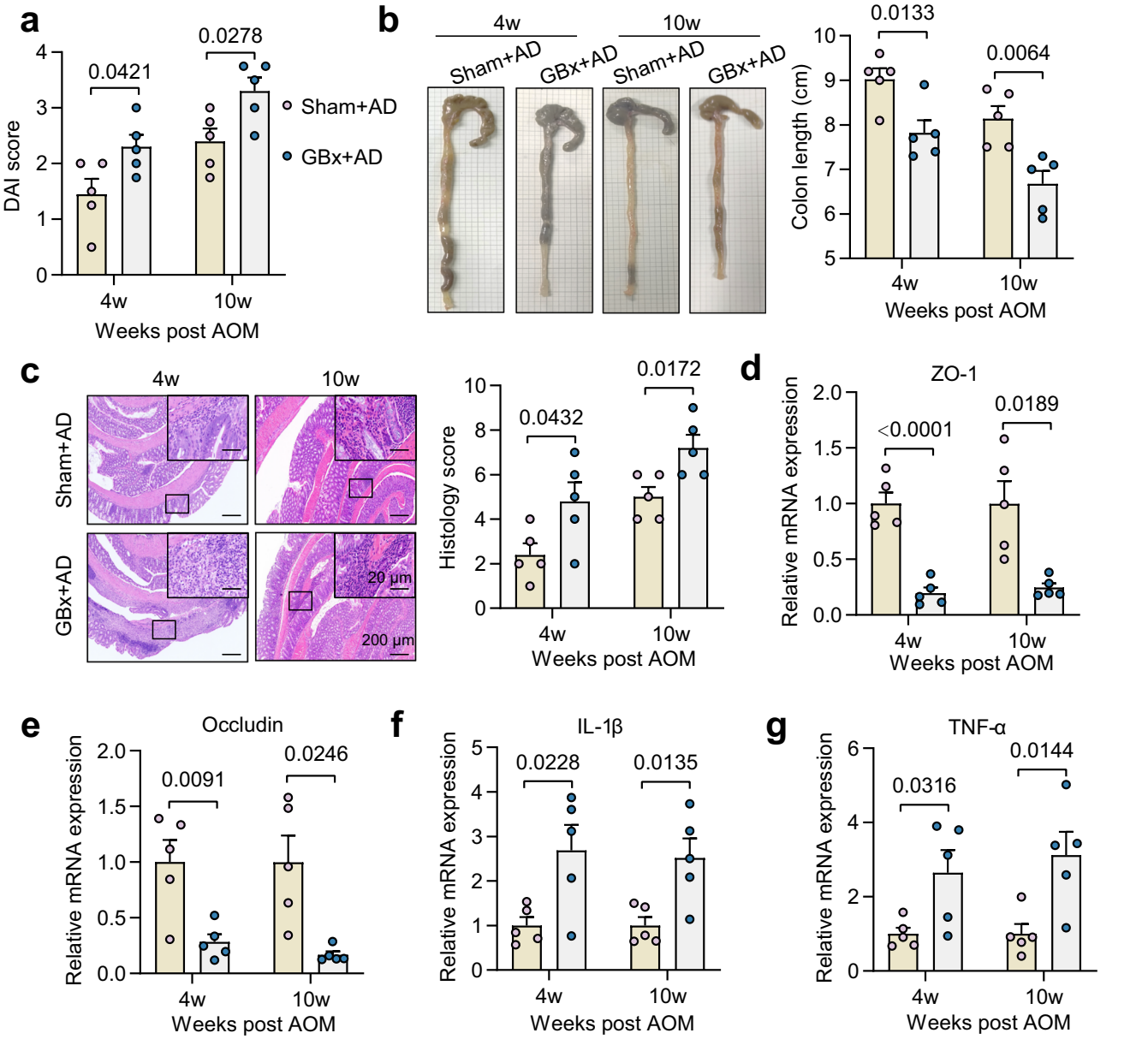

Fig. 2 | Cholecystectomy exacerbates colitis in AOM/DSS mouse model. a DAI score of Sham+AOM/DSS and GBx+AOM/DSS mice at week 4 and 10 after AOM injection. **b** Representative macrograph of colons and colon length. **c** H&E staining of colon tissue (left) and histological score (right). Histological slides showed acute inflammation at 4 weeks and chronic inflammation at 10 weeks following AOM injection. The bottom scale bar is 200 μm, and the top scale bar is 20 μm. **d**–**g** Relative expression of ZO-1 (**d**), Occludin (**e**), IL-1β (**f**) and TNF-α (**g**) in colonic tissues. $n = 5$/group. Data are shown as the mean ± SEM. *P* values were determined by a two-tailed *t* test and were indicated in each figure. DAI, disease activity index; ZO-1, tight junction protein 1; IL-1β, interleukin-1β; TNF-α, tumor necrosis factor alpha. All data are representative of more than three independent experiments. Source data are provided as a Source Data file.

significantly increased (Fig. 4g–j). To further verify that the abundance change is attributed to cholecystectomy, we tested the levels of these two bacteria in the GBx model and the APC-GBx mice model. Consistently, the abundance of *B. breve* significantly decreased, and the abundance of *R. gnavus* significantly increased (Fig. 4k–n) in these two mice models. And the abundance of *B. breve* and *R. gnavus* did not differ significantly between the two groups at baseline (Supplementary Fig. 8c, d), suggesting that in the AOM/DSS and $APC^{min/+}$ models, the alterations in bacteria are caused by cholecystectomy. Moreover, after fecal transplantation, the abundance of *B. breve* in the FMT-GBx group was much lower (Supplementary Fig. 8e), while the abundance of *R. gnavus* was much higher (Supplementary Fig. 8f), compared to FMT-HC group. In addition, the abundance of *B. breve* in FMT-GBx group was reduced (Supplementary Fig. 8g), while the abundance of *R. gnavus* was increased (Supplementary Fig. 8h), compared to the FMT-Sham group. Therefore, our data indicate that cholecystectomy can reduce the level of *B. breve* and increase the level of *R. gnavus*.

B. breve and *R. gnavus* control colorectal tumorigenesis through GUDCA and TUDCA production

To investigate the role of *B. breve* and *R. gnavus* in colorectal tumorigenesis, mice were gavaged with *B. breve* or *R. gnavus* (Supplementary Fig. 9a), and successful colonization of *B. breve* and *R. gnavus* was confirmed (Supplementary Fig. 9b, c). Mice gavaged with *B. breve* exhibited a decrease in tumor number (Supplementary Fig. 9d), a decrease in histopathological grading (Supplementary Fig. 9e) and decreased levels of serum markers (Supplementary Fig. 9f, g). In contrast, gavage with *R. gnavus* promoted colorectal tumorigenesis (Supplementary Fig. 9d, e) and increased the levels of CEA and CA19-9 (Supplementary Fig. 9f, g).

https://doi.org/10.1038/s41467-025-62956-8

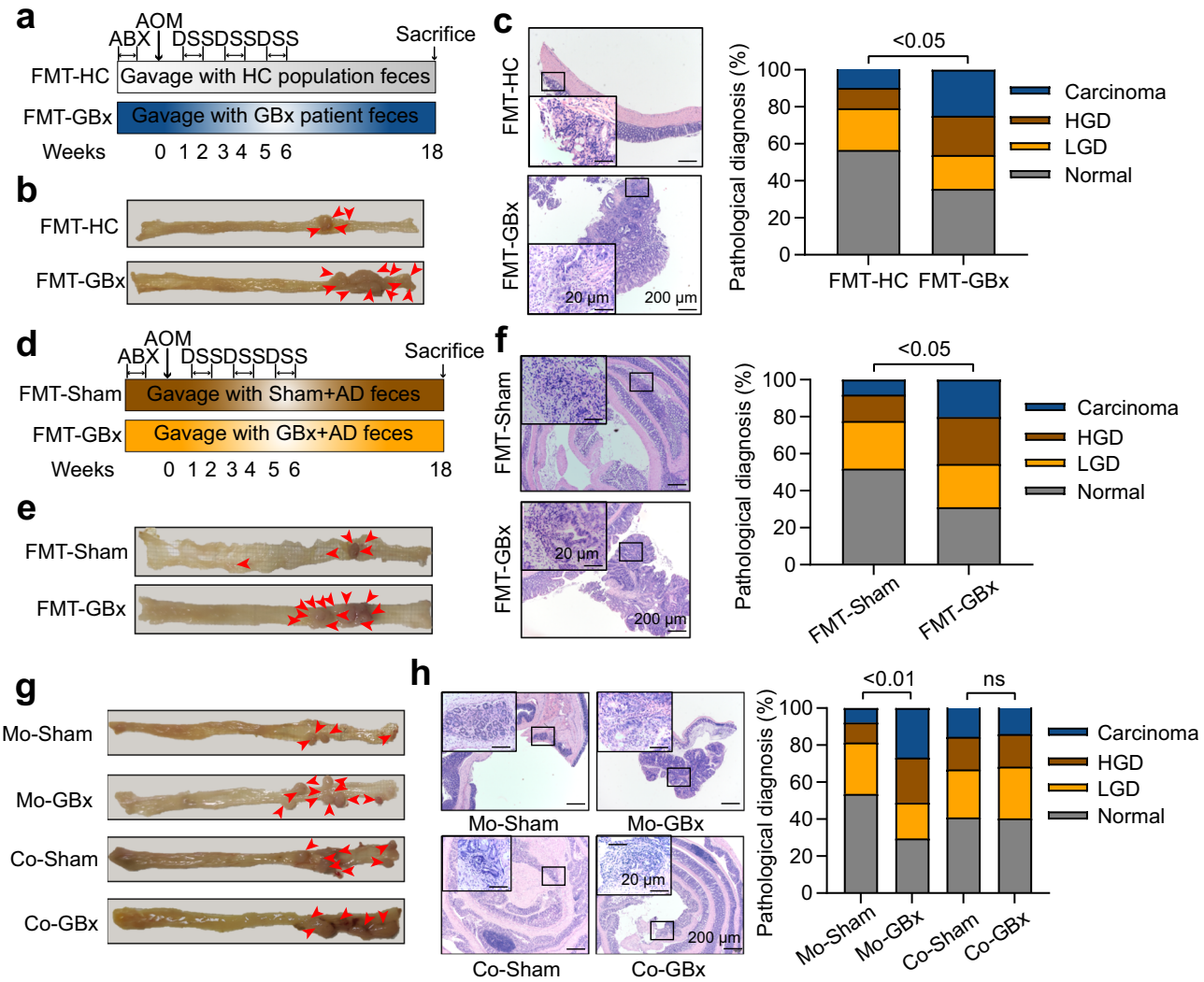

Fig. 3 | Cholecystectomy exacerbates colorectal tumorigenesis in a gut microbiota-dependent manner. a Experimental design for patient FMT mouse model. **b** Representative images of mouse colons ($n = 6$/group). **c** Representative images of H&E staining (left) and semiquantitative analysis (right) ($n = 6$/group). H&E staining presented normal mucosa, dysplastic mucosae, and carcinoma in the colon tissues. **d** Schematic overview of mouse fecal FMT model. **e** Representative images of the colon ($n = 5$/group). **f** Representative images of H&E staining (left) and semiquantitative analysis (right) ($n = 5$/group). H&E staining showed normal, dysplastic mucosae and carcinoma in the colon tissues. **g** Representative images of the colon in the cohousing experiments ($n = 7$/group). **h** Representative images of H&E staining (left) and semiquantitative analysis (right) in each group ($n = 7$/group). H&E staining showed normal, dysplastic mucosae and carcinoma in the colon tissues. The bottom scale bar is 200 μm and the top scale bar is 20 μm for **c, f**, and **h**. Data are shown as the mean ± SEM. *P* values were determined by ANOVA. ns not significant, FMT fecal microbiota transplantation, Mo mono-housed, Co co-housed. Source data are provided as a Source Data file.

Importantly, the growth of *B. breve* was inhibited in bile salts in a concentration-dependent manner (Supplementary Fig. 10a), while *R. gnavus* was resistant to bile salts (Supplementary Fig. 10b). We subsequently investigated the changes in bile acids in cholecystectomy patients. The fecal total bile acid level remained unchanged (Supplementary Fig. 11a), whereas, the serum total bile acid level was much higher in patients with cholecystectomy (Supplementary Fig. 11b). The ratio of conjugated bile acids to unconjugated bile acids increased (Supplementary Fig. 11c). Furthermore, quantitative analysis of fecal bile acids indicated that several bile acids were elevated in the cholecystectomy group (Supplementary Fig. 11d). Z-score analysis showed that the relative level of GUDCA presented the most significant difference between the two groups (Supplementary Fig. 11e). These results suggest that the bile acid levels were altered after cholecystectomy. We then performed bile acid profiling of fecal samples in C57BL/6 J mice with or without AOM/DSS administration and in $APC^{min/+}$ mice. Here, we found that there was no significant change in the total bile acid levels (Supplementary Fig. 12a), while the ratio of conjugated bile acids to unconjugated bile acids increased after cholecystectomy without AOM/DSS treatment (Supplementary Fig. 12b). Moreover, the level of TUDCA and several bile acids was increased after cholecystectomy (Supplementary Fig. 12c). After AOM/DSS treatment, there was no significant change in the total bile acid levels (Supplementary Figs. 13a and 14a), while the ratio of conjugated bile acids to unconjugated bile acids increased (Supplementary Figs. 13b and 14b). Furthermore, cholecystectomy resulted in higher levels of TUDCA in both AOM/DSS and APC genetic manipulation mouse models (Supplementary Figs. 13c and 14c). Moreover, no significant difference was detected in the fecal TUDCA level between the Sham group and the APC-Sham group (Supplementary Fig. 14d), indicating that cholecystectomy could change the fecal TUDCA levels in both AOM/DSS and $APC^{min/+}$ models. We further measured the levels of bile acids in distal ileum, serum, and liver after GBx with AOM/DSS treatment. The total bile acids (Supplementary Fig. 15a) and the ratio of conjugated to unconjugated bile acids (Supplementary Fig. 15b) were significantly increased in the ileum. Meanwhile, the level of TUDCA and several bile

https://doi.org/10.1038/s41467-025-62956-8

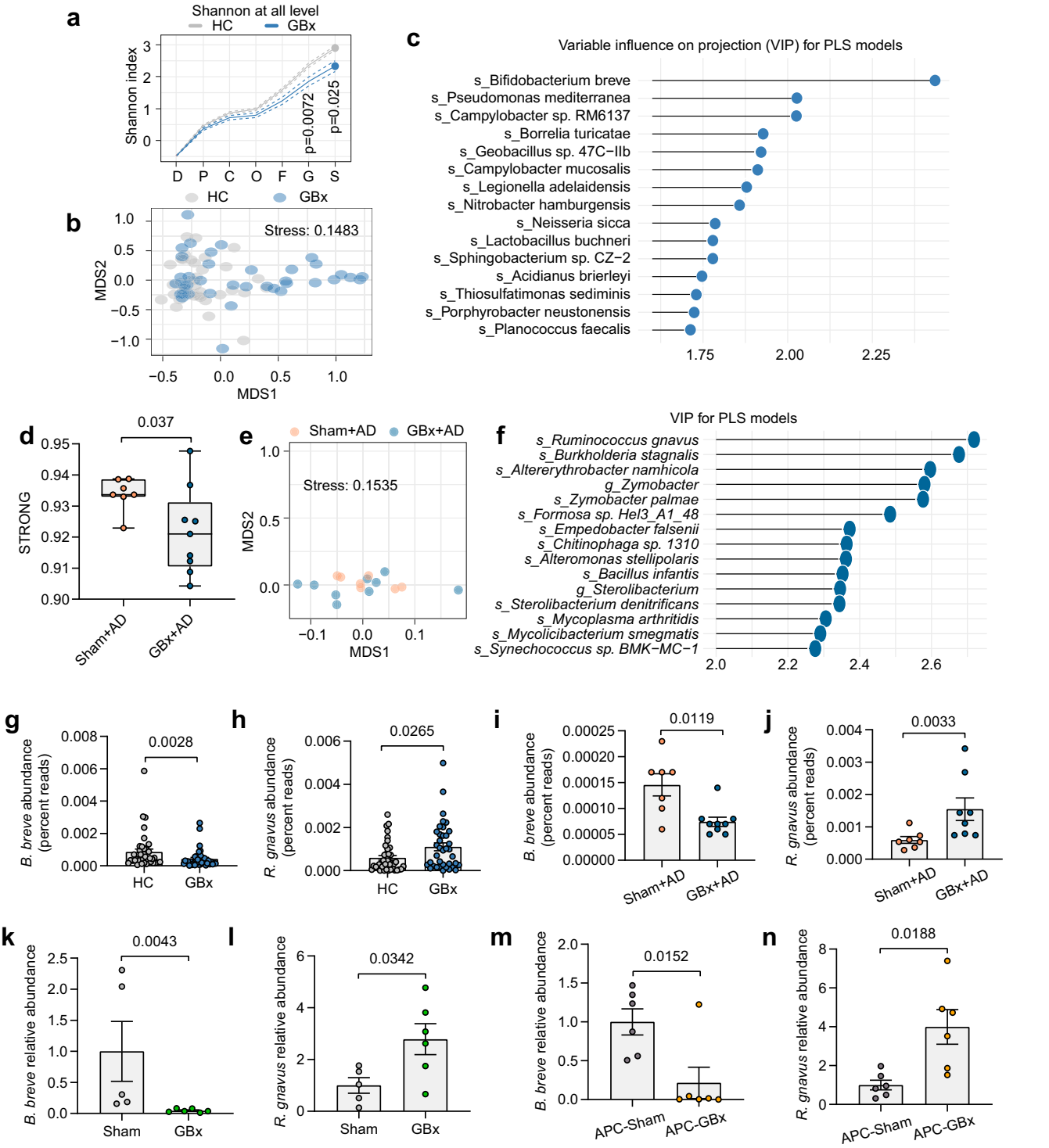

acids in the ileum was increased (Supplementary Fig. 15c). Consistently, the total bile acids were increased in the serum (Supplementary Fig. 15d), with no significant difference in the ratio of conjugated to unconjugated bile acids (Supplementary Fig. 15e). Additionally, there was no significant change in total bile acids and the ratio of conjugated to unconjugated bile acids in the liver between the two groups (Supplementary Fig. 15f, g).

We subsequently detected alterations in the fecal bile acid profiles in mice following intragastric administration of a single bacteria. Mice gavaged with *B. breve* exhibited a marked reduction in the TUDCA level, which was elevated in mice gavaged with *R. gnavus* (Fig. 5a). The ratio of conjugated to unconjugated bile acids was significantly reduced in *B. breve*-gavaged mice (Fig. 5b), while the ratio of secondary to primary bile acids was significantly increased in *R. gnavus*-gavaged mice (Fig. 5c). To verify whether GUDCA or TUDCA in the absence of cholecystectomy could reproduce the effect of cholecystectomy on CRC oncogenesis, we conducted a gavage experiment (Supplementary Fig. 16a). We measured the levels of GUDCA or TUDCA in feces after gavage of GUDCA or TUDCA in the absence of cholecystectomy. The data showed that the fecal levels of GUDCA or TUDCA increased significantly (Supplementary Fig. 16b, c), and were comparable to the fecal levels of TUDCA after cholecystectomy. Subsequently, we observed that TUDCA or GUDCA treatment in the absence of cholecystectomy could develop an increased number of tumors

Fig. 4 | The gut microbiota profiles in cholecystectomy patients and mice models. a α-diversity of the gut microbiota at all levels in HC and GBx patients (two-tailed Welch's *t* test). **b** NMDS of bacterial communities based on Bray-Curtis similarity. **c** VIP score of the PLS-DA in gut microbiota. VIP scores were used to rank the ability of different taxa to discriminate between the two groups. A taxon with VIP score > 2.0 was considered important in the discrimination. **d** Index (α-diversity) of the gut microbiota between Sham+AOM/DSS and GBx+AOM/DSS mice. (two-tailed Welch's *t* test, $n = 7$ vs 9). The center line of the boxplot represents the median; the box spans from the first quartile (Q1) to the third quartile (Q3); the whiskers extend from the box to the maximum and minimum values within 1.5 times the interquartile range (IQR) from the box. **e** NMDS of bacterial communities based on Bray-Curtis similarity ($n = 7$ vs 9). **f** VIP score of the PLS-DA. VIP scores were used to rank the ability of different taxa to discriminate between the two groups. A taxon with VIP score > 2.0 was considered important in the discrimination ($n = 7$ vs 9). **g** Relative abundance (percent reads) of *B. breve* between healthy and cholecystectomy patients based on metagenomics sequencing. **h** Relative abundance (percent reads) of *R. gnavus* between healthy and cholecystectomy patients based on metagenomics sequencing. **i** The relative abundance of *B. breve* between the Sham+AD and GBx+AD group ($n = 7$ vs 9). **j** Relative abundance of *R. gnavus* between Sham+AOM/DSS and GBx+AOM/DSS mice ($n = 7$ vs 8). **k** qPCR analysis of *B. breve* abundance in Sham and GBx mice ($n = 5$ vs 6). **l** qPCR analysis of *R. gnavus* in Sham and GBx mice (two-tailed *t* test, $n = 5$ vs 6). **m** qPCR analysis of *B. breve* abundance in APC-Sham and APC-GBx mice ($n = 6$/group). **n** qPCR analysis of *R. gnavus* in $APC^{min/+}$ mice (two-tailed Welch's *t* test, $n = 6$/group). Data are shown as the mean ± SEM. *P* values were determined by two-tailed Mann-Whitney *U* test for **g**–**k, m**, and were indicated in each figure. HC healthy control, AD AOM/DSS, NMDS nonmetric multidimensional scaling, VIP variable importance in projection, *B. breve*, *Bifidobacterium breve*, *R. gnavus Ruminococcus gnavus*. Source data are provided as a Source Data file.

(Supplementary Fig. 16d), a higher histopathological grading (Supplementary Fig. 16e), and increased levels of CEA and CA19-9 (Supplementary Fig. 16f, g). These results suggest that gavage of either GUDCA or TUDCA in the absence of cholecystectomy can also promote the development of CRC.

As conjugated bile acid mainly exists in the glycine form in humans and in the taurine form in mice[13], we previously observed a significant increase in the level of GUDCA in patients with cholecystectomy and TUDCA in a mouse model with cholecystectomy. Thus, we then used GUDCA for subsequent experiments to better simulate the role of bile acids in humans. To clarify whether the accumulation of GUDCA after cholecystectomy is due to the inhibition of bile salt hydrolase (BSH) activity caused by *B. breve*, we conducted the BSH activity assay. The deconjugation of GUDCA was significantly increased by *B. breve* administration (Fig. 5d), and *B. breve* was negatively correlated with GUDCA in patients with cholecystectomy (Supplementary Fig. 17a). Moreover, GBx+AOM/DSS mice had lower total BSH activity (Fig. 5e). *R. gnavus* can participate in the formation of GUDCA and TUDCA through 7β-hydroxysteroid dehydrogenase (7β-HSDH) activity[14,15]. Moreover, we observed a high 7β-HSDH activity in *R. gnavus* for the production of GUDCA (Fig. 5f). Besides, *R. gnavus* was positively correlated with the TUDCA levels in mice (Supplementary Fig. 17b), and GUDCA levels in cholecystectomy patients (Supplementary Fig. 17c). In addition, the total 7β-HSDH activity in GBx+AOM/DSS mice (Fig. 5g) was increased. These results suggested that decreased BSH activity due to *B. breve* reduction and increased 7β-HSDH activity by *R. gnavus* accumulation might contribute to the production of GUDCA after cholecystectomy.

In order to explore the role of bacterial BSH and HSDH activity in cholecystectomy-mediated colorectal tumorigenesis, we used BSH inhibitor riboflavin and 7β-HSDH inhibitor UDCA, respectively. Notably, gavage with *B. breve* reduces the fecal TUDCA level, while riboflavin can increase the *B. breve*-mediated TUDCA level (Supplementary Fig. 17d). Moreover, UDCA treatment can reverse the elevation of TUDCA levels mediated by *R. gnavus* (Supplementary Fig. 17e). *B. breve* administration significantly mitigated cholecystectomy-induced colorectal tumors and tumor pathology, which was reversed by the BSH inhibitor riboflavin (Fig. 5h, i and Supplementary Fig. 18a, b). The tumor number, the proportion of adenocarcinoma and high-grade dysplasia in mice were significantly increased after *R. gnavus* administration, which was reversed by the 7β-HSDH inhibitor UDCA (Fig. 5h, i and Supplementary Fig. 18a, b). We then measured the impact of UDCA supplementation on fecal bile acid levels in our model. In mice treated with UDCA, there was a significant increase in the levels of UDCA and its metabolite LCA (Supplementary Fig. 18c). Additionally, UDCA supplementation led to an elevation in the level of unconjugated bile acids, while the level of conjugated bile acids remained unchanged (Supplementary Fig. 18d). Furthermore, administration of GUDCA was able to increase the number of colorectal tumors (Fig. 5j and Supplementary Fig. 18e) and the pathological grading (Fig. 5k and Supplementary Fig. 18f). Similarly, we observed that TUDCA could also increase colorectal tumors (Fig. 5j and Supplementary Fig. 18e) and tumor pathology (Fig. 5k and Supplementary Fig. 18f). Taken together, these results indicate that the reduction in *B. breve* after cholecystectomy curtails the deconjugation of GUDCA and TUDCA via its BSH activity, while the increase in *R. gnavus* promotes the production of GUDCA and TUDCA through its 7β-HSDH activity; the augmented level of GUDCA and TUDCA then gives rise to colorectal tumorigenesis.

FXR/β-catenin signaling is involved in cholecystectomy-induced colorectal tumorigenesis

To further investigate the specific mechanism underlying cholecystectomy-induced colorectal tumorigenesis, RNA-seq analysis was performed using the colon cancerous tissues in Sham+AOM/DSS and GBx+AOM/DSS group, respectively. In the GBx+AOM/DSS group, 213 genes were upregulated and 542 genes were downregulated (Fig. 6a). As shown in Fig. 6b, cholecystectomy inhibited FXR signaling. We further observed that the expression of FXR (Fig. 6c) and its downstream gene SHP (Fig. 6d) was significantly decreased in the GBx+AOM/DSS group, while the expression of other bile acid receptors, PXR, TGR5 and VDR (Supplementary Fig. 19a–c), exhibited no significant alterations. Moreover, the expression of FXR and SHP (Supplementary Fig. 19d, e) was decreased in the GBx group without AOM/DSS treatment. As shown in Fig. 6e, KEGG analysis indicated that the Wnt signaling pathway was involved in this model. The expression of MYC (Fig. 6f) in the GBx+AOM/DSS group was higher, while no changes were found in other Wnt/β-catenin target genes (Supplementary Fig. 20a–e). Moreover, the expression of MYC (Supplementary Fig. 20f) was increased after GBx without AOM/DSS treatment. FXR expression was significantly suppressed while β-catenin and c-Myc were increased after GBx+AOM/DSS treatment (Fig. 6g). The immunofluorescence results showed that the β-catenin expression was much higher in the GBx+AOM/DSS group (Fig. 6h). In addition, the immunohistochemical results further confirmed that, FXR expression was decreased, while β-catenin and c-Myc were significantly increased in the GBx+AOM/DSS group (Fig. 6i and Supplementary Fig. 21a–c).

FXR is predominantly located in the nucleus, and it has been reported that FXR interacts with β-catenin to form a complex, which subsequently interferes with the transcriptional activity of the β-catenin/TCF complex[16]. Co-IP analysis of nuclear lysates showed a decreased association of FXR with β-catenin in GBx+AOM/DSS group (Fig. 6j). Moreover, reverse IP with β-catenin antibody likewise showed reduced association with FXR (Fig. 6j). However, the binding of β-catenin and TCF4 increased significantly after GBx+AOM/DSS treatment (Fig. 6k). As shown in Supplementary Fig. 21d, FXR knockdown could increase β-catenin luciferase intensity. In addition, FXR knockdown significantly enhanced the cell viability, which could be reversed by the Wnt signaling inhibitor XAV-939 (Supplementary Fig. 21e). Therefore, FXR is inhibited

https://doi.org/10.1038/s41467-025-62956-8

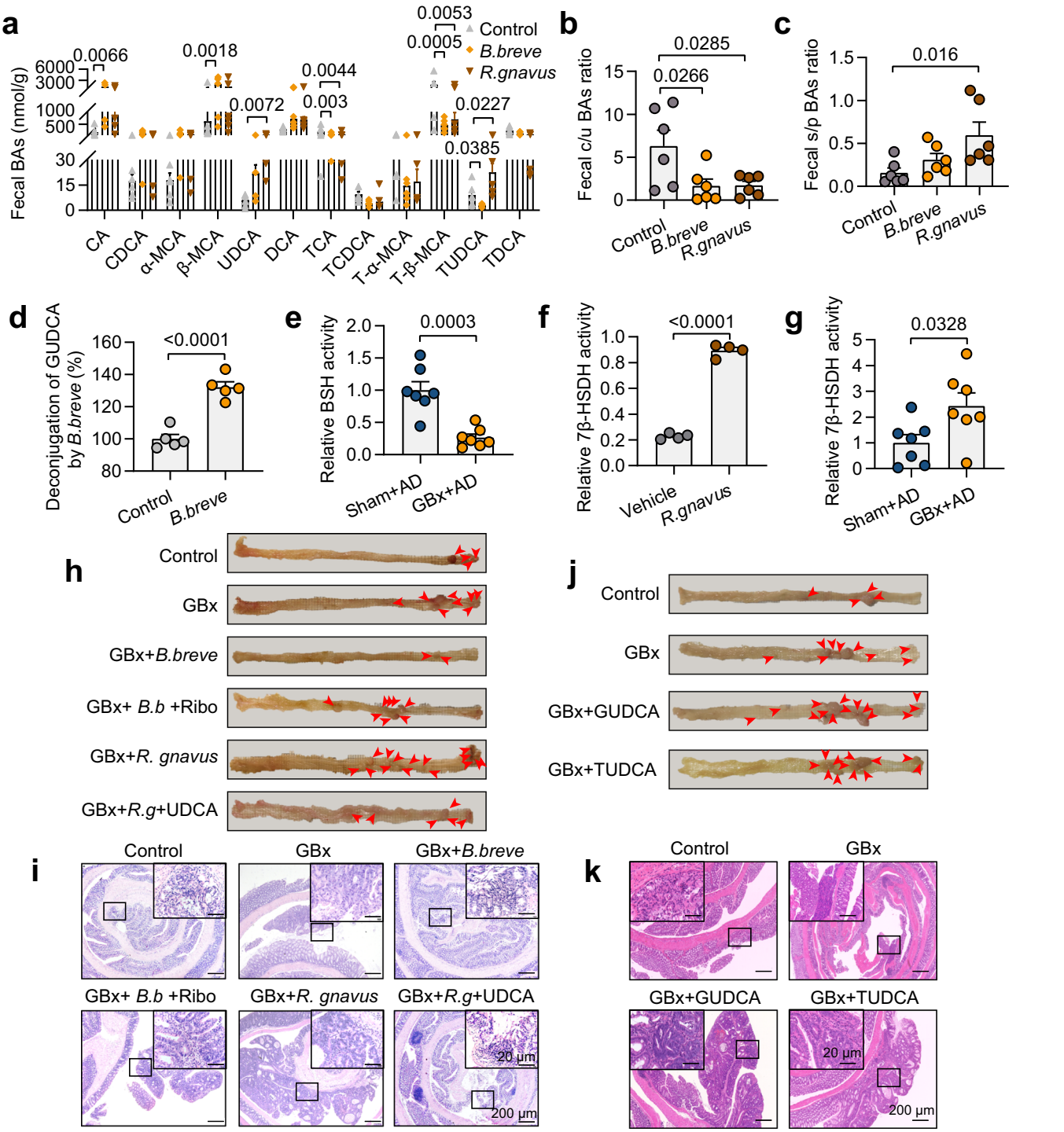

Fig. 5 | *B. breve*- and *R. gnavus*-mediated bile acid metabolism is involved in colorectal tumorigenesis. a Individual bile acid levels of mice gavaged with control, *B. breve* or *R. gnavus* ($n = 6$/group). **b** The ratio of conjugated to unconjugated bile acids in feces ($n = 6$/group). **c** The ratio of secondary to primary bile acids in feces ($n = 6$/group). *P* values were determined by ANOVA for **a**-**c**. **d** The hydrolysis efficiency of GUDCA mediated by *B. breve* ($n = 5$/group). **e** Relative BSH activity of Sham+AOM/DSS and GBx+AOM/DSS mice ($n = 7$/group). **f** The activity of 7β-HSDH mediated by *R. gnavus* ($n = 4$/group). **g** Relative 7β-HSDH activity of Sham+AOM/DSS and GBx+AOM/DSS mice ($n = 7$/group). *P* values were determined by two-tailed *t* test for **d**–**g**. **h, i** Representative images of mouse colon (**h**) and H&E staining (**i**). Mice were gavaged with *B. breve* or *R. gnavus* and then treated with BSH inhibitor riboflavin or 7β-HSDH inhibitor UDCA, respectively ($n = 7$/group). H&E staining showed normal, dysplastic mucosae and carcinoma in the colon tissues. The bottom scale bar is 200 μm and the top scale bar is 20 μm. **j, k** Representative images of mouse colon (**j**) and H&E staining (**k**). Mice were treated with GUDCA or TUDCA after the AOM/DSS model was established ($n = 8$/group). H&E staining showed normal, dysplastic mucosae and carcinoma in the colon tissues. The bottom scale bar is 200 μm and the top scale bar is 20 μm. Data are shown as the mean ± SEM. *P* values are indicated in each figure. AD: AOM/DSS; *B. breve*, *Bifidobacterium breve*; *R. gnavus*, *Ruminococcus gnavus*; BSH bile salt hydrolase, BAs bile acids, c/u BAs, conjugated to unconjugated bile acids, s/p BAs secondary to primary bile acids; 7β-HSDH, 7β-hydroxysteroid dehydrogenase, UDCA ursodeoxycholic acid, Ribo riboflavin. Source data are provided as a Source Data file.

https://doi.org/10.1038/s41467-025-62956-8

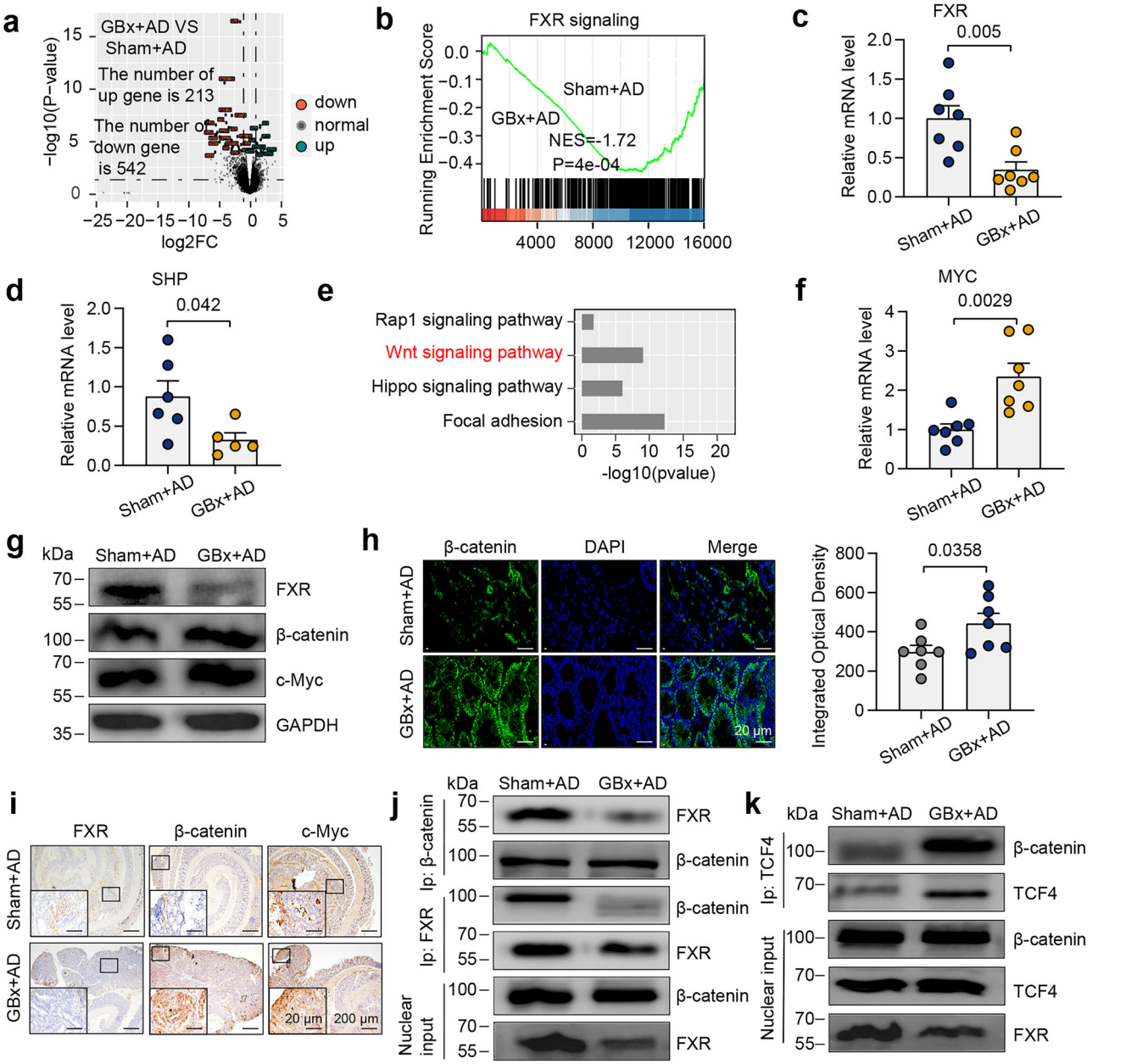

Fig. 6 | FXR/β-catenin signaling is involved in cholecystectomy-related colorectal tumorigenesis. a Volcano plot of RNA-seq analysis of colon cancerous tissue. The upregulated genes (green) and the downregulated genes (red) with a fold change <0.6 ($n = 3$/group) were shown. *P* values were adjusted by Benjamini & Hochberg (BH) method to control FDR. FDR-adjusted P < 0.05 was shown. **b** GSEA of the changes in the FXR pathway genes between Sham+AOM/DSS and GBx+AOM/DSS group ($n = 3$/group). Negative NES indicates that the level is lower in GBx +AOM/DSS group. **c** Relative expression of FXR in colon cancerous tissues ($n = 7$/group). **d** Relative expression of SHP in colon cancerous tissues ($n = 6$ vs 5). **e** KEGG pathway analysis of Sham+AOM/DSS and GBx+AOM/DSS mice ($n = 3$/group). *P* values were adjusted by BH method to control FDR. FDR-adjusted P < 0.05 was shown. **f** Relative expression of MYC in colon cancerous tissues ($n = 7$/group). **g** Western blot analysis of FXR, β-catenin, c-Myc, and GAPDH within the colon cancerous tissues from Sham+AOM/DSS and GBx+AOM/DSS mice. GAPDH was used as a loading control. **h** Immunofluorescence analysis of β-catenin ($n = 7$/group). β-Catenin, green; DAPI, blue. Scale bar, 20 μm. **i** Representative image of IHC staining of FXR, β-catenin, and c-Myc ($n = 7$/group). The bottom scale bar is 200 μm and the top scale bar is 20 μm. **j** Co-immunoprecipitation analysis of the interaction between FXR and β-catenin in colon cancerous tissues. **k** Co-IP of the interaction between TCF4 and β-catenin in colon cancerous tissues. Data are shown as the mean ± SEM. *P* values were determined by two-tailed *t* test and were indicated in each figure. FXR farnesoid X receptor, SHP small heterodimer partner, TCF transcription factor. All data are representative of more than three independent experiments. Source data are provided as a Source Data file.

after cholecystectomy, and the binding of FXR and β-catenin would decrease, thereby increasing the binding of β-catenin and TCF4, and ultimately promoting the colorectal tumorigenesis.

OCA suppressed cholecystectomy-associated colorectal tumorigenesis

We employed OCA, a commercial agonist of FXR, to treat mice with cholecystectomy in AOM/DSS model (Fig. 7a). The colorectal tumor number was significantly increased after GBx, whereas OCA dramatically decreased the tumor number (Fig. 7b, c). Histological examination showed the reduced proportions of adenocarcinoma and high-grade dysplasia in OCA-treated mice (Fig. 7d), along with the reduced intestine permeability (Supplementary Fig. 22a) and decreased levels of CEA and CA19-9 (Supplementary Fig. 22b, c). In addition, we observed that after cholecystectomy, the expression of FXR and SHP decreased, the expression of β-catenin and c-Myc increased, the

https://doi.org/10.1038/s41467-025-62956-8

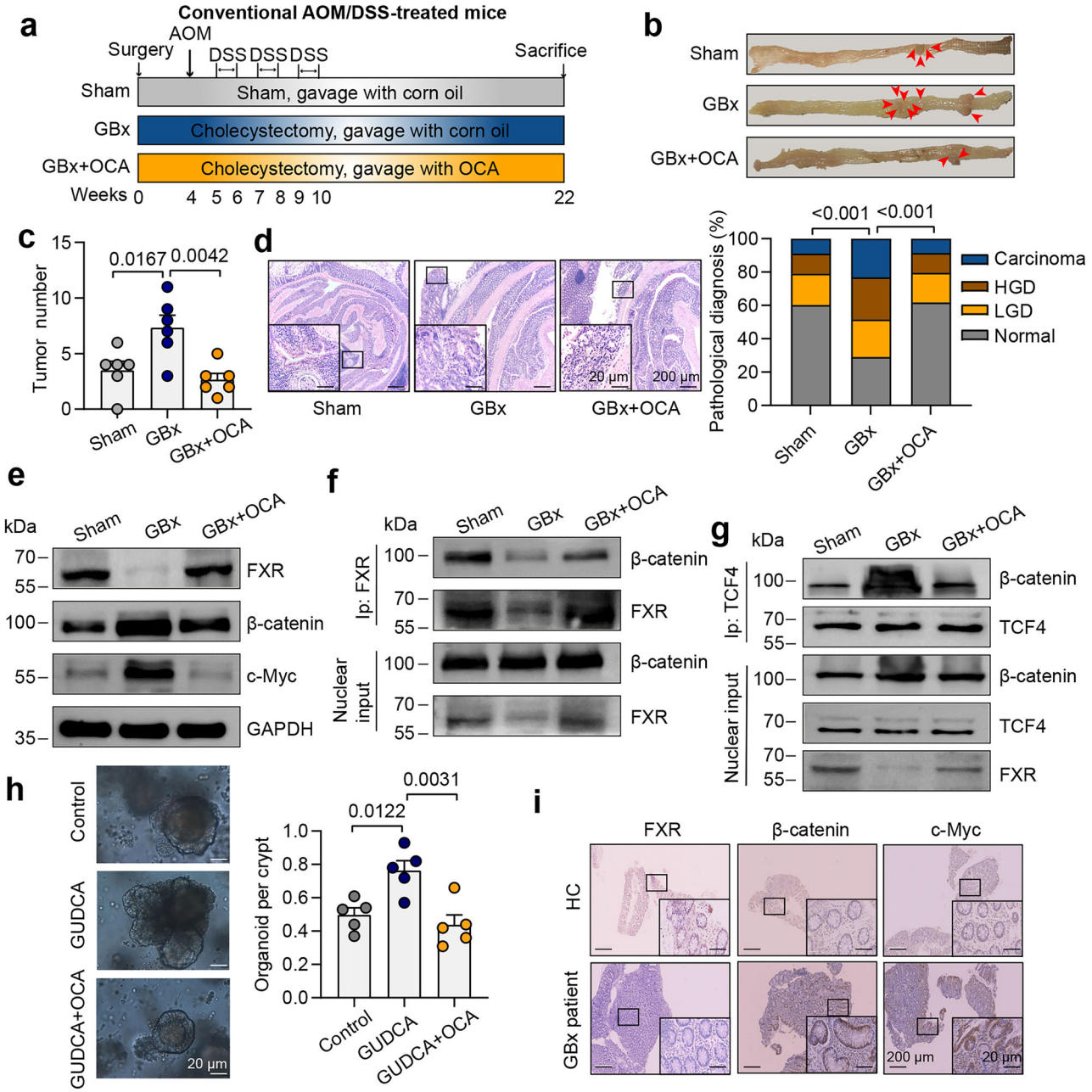

Fig. 7 | OCA prevents cholecystectomy-induced colorectal tumorigenesis. **a** Schematic overview shows OCA treatments in the sham or cholecystectomy mice with AOM/DSS treatment. **b** Representative images of the colon ($n = 6$/group). **c** Average tumor number ($n = 6$/group). **d** Representative images of H&E staining (left) and semiquantitative analysis (right) ($n = 6$/group). H&E staining showed normal, dysplastic mucosae and carcinoma in the colon tissues. The bottom scale bar is 200 μm and the top scale bar is 20 μm. **e** Protein expression of FXR, β-catenin, c-Myc, and GAPDH within the colon cancerous tissues for each group. **f** Co-immunoprecipitation of the interaction between FXR and β-catenin in colon cancerous tissues. **g** Co-immunoprecipitation of the interaction between TCF4 and β-catenin in colon cancerous tissues. **h** Representative image and quantification of organoids generated from GBx+AOM/DSS mice treated with control, GUDCA (100 μM), or GUDCA + OCA (10 μM) ($n = 5$/group). Scale bar, 20 μm. **i** IHC staining of FXR, β-catenin, and c-Myc in healthy controls and cholecystectomy patients in colon tissues. ($n = 4$/group). The bottom scale bar is 200 μm and the top scale bar is 20 μm. Data are shown as the mean ± SEM. *P* values were determined by ANOVA and were indicated in each figure. HC healthy control, GBx cholecystectomy, OCA obeticholic acid. Source data are provided as a Source Data file.

binding of FXR and catenin decreased, and the binding of β-catenin and TCF4 increased. These changes could be reversed by OCA (Fig. 7e–g and Supplementary Fig. 22d–f). Moreover, in non-tumor tissues, OCA can still reverse the decrease in the expression of FXR and the increase in β-catenin that were induced by GBx (Supplementary Fig. 22g). We then used the intestinal epithelial organoid model from GBx+AOM/DSS mice to examine the effects of OCA. Notably, OCA inhibited GUDCA-induced organoid growth (Fig. 7h). Mechanistically, we found that OCA could induce FXR and SHP (Supplementary Fig. 22h, i) expression, and down-regulate MYC expression (Supplementary Fig. 22j). Finally, we examined the changes of FXR/β-catenin signaling in patients with cholecystectomy. FXR expression was significantly reduced in cholecystectomy patients compared to the healthy controls group, while the expression of β-catenin and c-Myc was increased (Fig. 7i and Supplementary Fig. 22k–m). Collectively, these findings support a model in which FXR/β-catenin interaction is disrupted after cholecystectomy, which can be prevented by OCA treatment (Fig. 8).

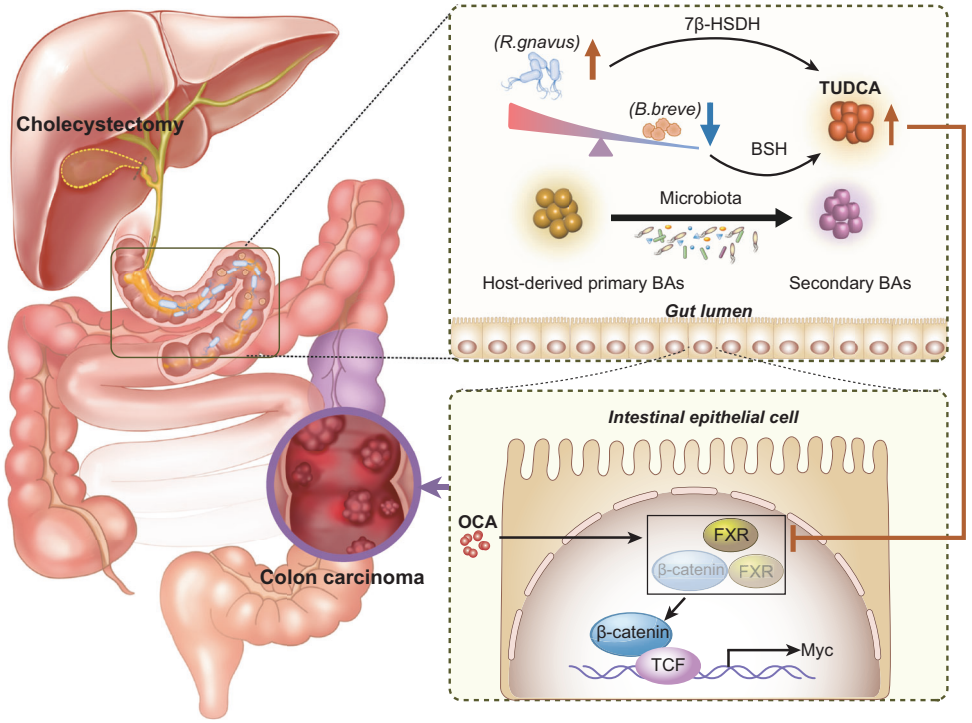

Fig. 8 | Conceptual diagram illustrating the potential interaction between cholecystectomy and colon carcinoma. Cholecystectomy can induce gut microbiota disorder, characterized by a significant decrease in the abundance of *B. breve* and an increase in the abundance of *R. gnavus*. The reduction in *B. breve* elevates the level of TUDCA via its BSH activity. Meanwhile, the augmented *R. gnavus* can promote the formation of TUDCA through its 7β-HSDH activity. TUDCA may ultimately lead to colon carcinoma by disrupting the interaction between FXR and β-catenin, which could further increase the binding of β-catenin and TCF4, thereby promoting MYC expression and facilitating colorectal tumorigenesis. OCA treatment may ultimately prevent colon carcinoma through FXR activation. The schematic was created using Adobe Illustrator 2024 (v28.7.0). *B. breve*, *Bifidobacterium breve*, *R. gnavus*, *Ruminococcus gnavus*; TUDCA tauroursodeoxycholic acid, 7β-HSDH 7β-hydroxysteroid dehydrogenase, BSH bile salt hydrolase, FXR farnesoid X receptor, TCF4 transcription factor 4, OCA obeticholic acid.

Discussion

Cholecystectomy is the most common procedure in biliary tract surgery, accompanied by long-term complications, such as recurrent choledocholithiasis and post-cholecystectomy syndrome[2]. Notably, previous meta-analysis showed that the risk of colon cancer after cholecystectomy was 30% higher[6]. Herein, we found that cholecystectomy-related perturbations in the gut microbiota promoted the production of GUDCA and TUDCA and facilitated colorectal tumorigenesis. Mechanistically, GUDCA and TUDCA inhibited FXR signaling, disrupted the FXR/β-catenin interaction, and ultimately exacerbated colorectal tumorigenesis, an effect that could be attenuated by OCA treatment.

Previous studies showed that the occurrence rate of CRC increased after cholecystectomy[5–7]. Here, we did find that 2 out of 52 patients after cholecystectomy developed CRC, implying an upward trend of CRC incidence after cholecystectomy. However, the difference we found in the incidence of CRC between cholecystectomized and healthy subjects was not significant, which could be explained by a small sample size. Notably, in our study, we found that cholecystectomy exacerbated the oncogenesis of CRC in both the AOM/DSS and $APC^{min/+}$ mouse models. It is well known that human colorectal cancer arises from the intricate interplay of both genetic and environmental factors. The $APC^{min/+}$ model predominantly serves to simulate genetically-driven CRC. In contrast, the AOM/DSS model operates through chemical induction. The mouse models were established to mimic certain aspects of CRC oncogenesis after cholecystectomy. Although they may not fully replicate the human situation, they provide valuable insights into the potential mechanisms. Importantly, we observed that cholecystectomy exacerbated early and late colitis in mice, and colorectal tumorigenesis developed much earlier after cholecystectomy. Given that the AOM/DSS model places great emphasis on inflammation-related carcinogenesis, we employed this model in the following study, which involved fecal microbiota transplantation, single bacterial colonization, and bile acid supplementation.

The gut microbiota constitutes the most significant microecosystem within the human body and is involved in a variety of physiological processes[17]. Numerous experiments have confirmed that the gut microbiota dysbiosis possesses a cancer-promoting effect[18]. We delineated the alterations in the gut microbiota subsequent to cholecystectomy, and found that cholecystectomy led to a decrease in the number of the key bacterium *B. breve* and an increase in the amount of *R. gnavus* in both the population after cholecystectomy and cholecystectomized mice. We then confirmed that *B. breve* was able to inhibit colorectal tumorigenesis, whereas *R. gnavus* could promote colorectal tumorigenesis through modulation of bile acid metabolism.

Under normal circumstances, the gallbladder plays a key role in regulating physiological homeostasis by controlling the rate and flow of bile into the intestine[19]. However, the rhythm of bile acid entering the intestine is changed after cholecystectomy. Moreover, the adaptation of bile acid metabolism may occur in patients post-cholecystectomy. Numerous studies have reported a significant increase in serum bile acid levels in patients who have undergone cholecystectomy[4,20], which is consistent with our results. After cholecystectomy, the increase in serum bile acid levels can be attributed to several factors. Firstly, removing the gallbladder disrupts the normal circulation and metabolism of bile acids, which changes their distribution in the body, directly causing a rise in serum bile acid levels[21,22]. Secondly, cholecystectomy interrupts the enterohepatic circulation of bile acids, leading to changes in the expression of genes related to bile acid synthesis. Concurrently, enhanced intestinal absorption of bile acids may occur, resulting in elevated serum bile acid levels[4,19]. Finally, after cholecystectomy, the continuous flow of bile into the intestine causes intestinal flora dysbiosis, which in turn affects the metabolism

and reabsorption of bile acids, leading to an increase in serum bile acid levels[8,23,24]. Moreover, we found that there was a significant increase in the ratio of conjugated to unconjugated bile acids, and several conjugated bile acids were increased after cholecystectomy. Although certain studies reported changes in serum DCA level, a substantial number of studies revealed that in both short-term and long-term follow-ups, there were no alterations of the CA or DCA pools after cholecystectomy in the patients[25,26], implying the complexity in kinetics of bile acids post-cholecystectomy. Here, we observed an increase in GUDCA levels in patients after cholecystectomy, with GUDCA showing the most significant difference. Despite the potential complication of bile acid profiles due to concomitant AOM/DSS intervention or APC genetic manipulation, a consistent change of TUDCA was observed in different mouse models after cholecystectomy.

It is well known that the intestinal flora plays an important role in bile acid metabolism. The taurine-conjugated and glycine-conjugated bile acids uncouple to their respective unconjugated free forms through the BSH activity produced by the gut microbiota[27,28]. Notably, *Bifidobacterium* has been shown to be the largest source of BSH in the human intestine[29]. Herein, we found that the total BSH activity was significantly decreased after cholecystectomy. Moreover, the deconjugation of GUDCA was significantly increased by *B. breve* administration. Notably, gavage with *B. breve* reduces the fecal TUDCA level, while riboflavin can increase the TUDCA level mediated by *B. breve*. Importantly, BSH inhibitor riboflavin can significantly worsen *B. breve*-mediated colorectal tumorigenesis after cholecystectomy. Conjugated-CDCA is capable of being converted into conjugated-UDCA. In humans, conjugated-UDCA predominantly exists in the form of GUDCA, whereas in mice, it mainly presents as TUDCA[13]. The catalytic enzymes that play a major role in this transformation process are 7α- and 7β-HSDH, which are found in *Ruminococcus*[15]. Here, we observed that the total 7β-HSDH activity was significantly upregulated after cholecystectomy. *R. gnavus* could promote GUDCA production through its 7β-HSDH activity. Importantly, the 7β-HSDH inhibitor UDCA can reverse the elevation of TUDCA levels mediated by *R. gnavus*. And UDCA treatment significantly reverses *R. gnavus*-mediated tumorigenesis. And previous studies in both humans and mice have revealed that upon UDCA treatment, LCA becomes the most abundant colonic bile acid as a result of modification by intestinal bacteria[30–32]. In addition, we have measured the effect of UDCA supplementation on fecal bile acid levels and we found that the levels of UDCA and its metabolite LCA increased significantly, while no significant differences were observed in the levels of TUDCA. Accumulating evidence has demonstrated that bacteria-modified bile acids, which are not the main components in the digestive tract, assume significant roles in diverse diseases[33–35]. Importantly, previous studies revealed that GUDCA or TUDCA played vital roles in multiple metabolic diseases or tumor development[13,36–39]. Here, we found that both GUDCA and TUDCA in the absence of cholecystectomy could reproduce the effect of cholecystectomy on CRC oncogenesis; thus we believe that TUDCA or GUDCA could promote cholecystectomy-mediated colorectal tumorigenesis. Therefore, the decreased BSH activity due to *B. breve* reduction and the increased 7β-HSDH activity due to *R. gnavus* accumulation might contribute to the production of GUDCA and TUDCA, thus promoting the occurrence of CRC after cholecystectomy. While GUDCA levels were elevated in cholecystectomized individuals, their colorectal cancer incidence did not exhibit a significant increase. This observation may be attributed to factors such as a relatively small sample size and insufficient duration of GUDCA exposure. We will conduct a more in-depth investigation into this in further studies.

FXR plays vital roles in CRC oncogenic transformation[9,12], and its expression in colon polyps is reduced, particularly in colon adenocarcinoma[12]. We observed that FXR signaling was inhibited in cholecystectomy-mediated colorectal tumorigenesis. The silencing of FXR reduces its inhibition of the Wnt/β-catenin signaling, leading to CRC carcinogenesis[16]. And here we also found that β-catenin signaling was upregulated after cholecystectomy. The interaction between Wnt/β-catenin signaling and nuclear receptors has garnered considerable attention in cancer research[40]. Nuclear FXR has been reported to interact with β-catenin to form a complex, which subsequently interferes with the transcriptional activity of the β-catenin/TCF. Inhibition of FXR disrupts the binding of catenin to TCF4[16]. Our results showed that the binding of FXR and β-catenin decreased, while the binding of β-catenin and TCF4 increased after cholecystectomy. Thus, our study reveals a non-transcriptional mechanism of FXR in cholecystectomy-mediated colorectal tumorigenesis, whereby FXR expression was downregulated after cholecystectomy, the interaction of FXR/β-catenin was subsequently disrupted, thus Wnt/β-catenin signaling was activated to promote colorectal tumorigenesis.

GUDCA or TUDCA has been identified as natural antagonists of FXR, which could inhibit the expression level of FXR[39,41]. And we did observe that FXR expression decreased after cholecystectomy, and treatment with GUDCA significantly downregulated FXR expression in intestinal epithelial organoids. Therefore, the decreased interaction between FXR and β-catenin was at least partially attributed to the decreased FXR expression. On the other hand, the FXR co-IP results seem to show dramatically reduced β-catenin interactions after cholecystectomy despite similar pull down of FXR, implying that some alternative mechanism might also contribute to the decreased β-catenin interaction. Previous study showed that TUDCA or GUDCA were molecularly docked with the LBD of FXR, both were surrounded by amino acid residues like Arg331, Met265, His447 and Tyr369 in this domain[13]. And it has been reported that FXR can bind to β-catenin through the AF surface, disrupting the assembly of the core β-catenin/TCF4 complex[42]. Whether FXR binding to agonistic or antagonistic bile acids affects its binding to catenin has not been reported yet. Here, we computationally investigated the direct interaction between FXR and β-catenin by molecular docking. The FXR/ligand complex structures available in the PDB database were categorized into unliganded states (apo-FXR) and liganded states[43]. For the apo-FXR (PDB ID: 5Q0K) and β-catenin (PDB ID: 1JDH), the binding free energy was calculated to be −620.11 kcal/mol, primarily due to the formation of six stable hydrogen bonds through the AF surface (Supplementary Fig. 23a). In contrast, when TUDCA or GUDCA were docked into the antagonistic ligand state of FXR (PDB ID: 4WVD), the binding free energy increased to −458.34 and −467.14 kcal/mol, respectively. This reduction was attributed to a decrease in the number of hydrogen bonds (Supplementary Fig. 23b and c), indicating a weaker binding affinity. Thus, the conformational changes of FXR induced by antagonistic bile acids, such as TUDCA or GUDCA, may interrupt the interaction between FXR and β-catenin, which might also be a potential mechanism contributing to the decreased binding of FXR and β-catenin.

Previous research has indicated that OCA is able to activate the FXR[44] and significantly promotes FXR expression[12,45]. Here, we observed that cholecystectomy had a dramatic effect on FXR expression in colon cancerous tissues. Probably some other effects such as dedifferentiation in tumor tissues, might also have contributed to this effect. However, in non-tumor tissues, OCA can still reverse the decreased expression of FXR caused by cholecystectomy. Moreover, OCA was able to reverse FXR/β-catenin signaling induced by GUDCA. Thus, it is believed that cholecystectomy inhibited FXR expression through its antagonist TUDCA or GUDCA, which could be reversed by OCA.

Taken together, we discovered that cholecystectomy can cause gut microbiota dysbiosis, characterized by diminished abundance of *B. breve* and increased abundance of *R. gnavus*. The reduction in *B. breve* elevated GUDCA and TUDCA levels by curtailing the deconjugation of GUDCA and TUDCA via its BSH activity, while the increase of *R. gnavus* facilitated GUDCA and TUDCA formation through its 7β-HSDH activity. GUDCA and TUDCA exacerbate colorectal tumorigenesis by disrupting

the FXR/β-catenin interaction. OCA treatment may ultimately prevent colon carcinoma through FXR activation. This study might offer clinicians a promising prevention strategy for cholecystectomy-related colorectal cancer through modulation of the gut microbiota-bile acid-FXR axis.

Methods

Ethics statement and sample collection from cholecystectomy patients

All research protocols and procedures were been approved by the Medical Ethics Committee of the Second Affiliated Hospital of the Army Military Medical University (Approved No. AMUWEC201908301) and conducted in accordance with Helsinki Declaration. Written informed consent was obtained from all participants prior to study inclusion. And from August 2019 to July 2020, a total of 52 patients who underwent cholecystectomy were recruited in the Second Affiliated Hospital of the Army Medical University. Meanwhile, 45 gender- and age-matched individuals without any biliary diseases or tumors were selected as the healthy controls. Specifically, these healthy controls were recruited from individuals who underwent routine physical examinations at our hospital. All participants were required to avoid probiotics, antibiotics, alcohol and smoking at least 2 months prior to sampling. Fecal samples were collected from all enrolled populations in sterilized fecal collection tubes equipped with fecal stabilizers (Longsee microbial sampling protection Kit). Serum and colorectal tissue samples were also collected from all participants and preserved in ultra-low-temperature liquid nitrogen for subsequent analysis. And both groups of participants had their colorectal tissues collected by medical staff using sterile biopsy forceps during colonoscopy screening. No cash compensation was provided to the participants; however, all study-related registration fees and examination costs were covered by our research institution.

Reagents and antibodies

Azoxymethane (AOM) and dextran sodium sulfate (DSS) were purchased from MP Biomedicals (Shanghai) Co., Ltd. Antibodies used were as follows: FXR monoclonal antibody (Santa cruz, sc-25309), β-catenin monoclonal antibody (Proteintech, 66379-1-Ig), c-Myc monoclonal antibody (Abcam, ab32072), Ki67 monoclonal antibody (Cell Signaling Technology, 9449), TCF4 monoclonal antibody (MCE, HY-P80520), and GAPDH polyclonal antibody (Proteintech, 10494-1-AP).

Metagenomic analysis

Total microbial genomic DNA samples were extracted from the samples following the manufacturer's instructions of the DNeasy PowerSoil Kit (QIAGEN, Netherlands). Subsequently, whole-genome shotgun sequencing for fecal samples from both human individuals and mice was conducted on the Illumina NovaSeq 6000 platform provided by Novogene (Tianjin, China). Quality filtering of metagenomic reads was achieved with Trimmomatic software (V.0.39). Taxonomic annotation of the metagenome and abundance quantification were accomplished via MetaPhlAn (V.2.0). Functional annotations were performed with data files from the HMP Unified Metabolic Analysis Network 3.0 (HUMAnN 3.0). Finally, the R package (V.4.0) was used to compute the differences in the abundance of bacteria. Analysis of fecal shotgun metagenomic sequences was carried out to determine the abundance of candidate bacteria previously identified in fecal samples from both human and mouse sources.

RNA-seq analysis

Mouse colon cancerous tissues were used for RNA-seq analysis. RNA quality was confirmed using the Agilent 2100 bioanalyzer; RNA seq libraries were prepared from three bioreplicates per experimental condition, and sequenced on Illumina NovaSeq 6000 using barcode multiplexing and a 150 bp read length (Novogene, Beijing, China). Image analysis and base calling were performed using Illumina CASAVA-1.8.2. And fastqc was used to assess reading quality. The readings were aligned using STAR against reference genomes and transcription annotations. RSEM was used to quantify gene expression in the BAM file. Differentially expressed genes were determined using rsem-generate-data-matrix and rsem-run-ebseq commands. For GSEA, the standardized expression of the gene matrix from the RSEM results was used with the previously reported gene signatures, and GSEA was performed with the default Settings. The combined KEGG database was used to analyze the differences of biological processes and signal pathways.

Mice

The wild-type C57BL/6 J male mice were obtained from Beijing Vital River Laboratory Animal Technology Co., Ltd. (Cat.# 219). And $APC^{Min/+}$ mice were purchased from Gempharmatech Co., Ltd. (Cat.# T001457-1). Throughout our study, all mice were kept in the stable condition, which includes a constant temperature (20-23 °C) combined with a proper humidity (40%-50%) and a strict 12 h light/dark cycle. All of our experimental animals had free access to foods (Beijing Huafukang Biotechnology, 1022) and water and all animal experiments were conducted in accordance with the National Institutes of Health Guide for the Care and Use of Laboratory Animals, which were approved by the Institutional Animal Care and Use Committee of the Third Military Medical University (Approved No. AMUWEC20210156). The tumor size was maintained within the maximum dimensions permitted by the ethics committee (length, width, and height each ≤ 2.0 cm). These limits were strictly adhered to throughout all in vivo studies. In vivo experiments were terminated either at predefined time points or when mice reached humane endpoints, which included: >20% body weight loss, or the presence of severe distress symptoms (e.g., lethargy, impaired mobility). Mice were monitored daily, and once the above criteria were met, they were euthanized promptly in accordance with the approved protocols.

GBx mouse model

After a week of adaptive feeding, the mice were randomly divided into cholecystectomy group (GBx) and control group (Sham). In the cholecystectomy group, the bile was drained, the cystic duct was ligated, and the gallbladder was removed. The control group mice were sham-operated. One month after the operation, AOM/DSS modeling was performed as follows.

The AOM/DSS mouse model

To construct an AOM/DSS-induced CRC model, we chose the male mice by the random sampling method and gave them an intraperitoneal injection of 12.5 mg/kg AOM. After 7 days, they were treated with 2% DSS in their drinking water for one week and then rested for one week. Subsequently, this cycle was repeated three times. The mice were harvested 18 weeks after AOM injection.

$APC^{min/+}$ mouse model

8-week-old male $APC^{min/+}$ C57BL/6 mice at were exposed to the same cholecystectomy and sham operation. The mice were harvested at 8 weeks after operation in $APC^{min/+}$ model.

Antibiotic cocktail (ABX) experiment

In order to eliminate the gut microbiota, the antibiotic cocktail (neomycin sulfate 200 mg/kg, metronidazole 200 mg/kg, ampicillin 200 mg/kg, and vancomycin 100 mg/kg) was used five times a week.

Bacterial culture, preservation and growth

B. breve (ATCC 15700) was streaked onto a BBL medium plate for 3 days, at 37 °C, under anaerobic conditions. A single colony was selected and placed in BBL liquid medium for cultivation in a 37 °C

anaerobic incubator. Similarly, *R. gnavus* (ATCC 35913) was cultured in a 37 °C anaerobic incubator using ATCC® medium 1490. When the culture reached around OD = 0.8, we subcultured it into a new culture medium. 1 ml of culture containing 25% (v/v) glycerol was divided into 1.5 ml EP tubes, frozen quickly with liquid nitrogen, and stored at −80 °C. Then the bacteria were resuscitated by oscillating at 37 °C for 30 minutes. For bile salt assays, porcine bile extract, which includes conjugated bile salts containing GUDCA and TUDCA plus other bile salts, as well as non-conjugated bile salts containing cholic acid (CA) sodium salt and deoxycholic acid (DCA) sodium salt, was added at final amounts of different concentrations (wt/vol) to both *B. breve* and *R. gnavus* cultures. *B. breve* and *R. gnavus* were cultured in anaerobic tubes and tested for OD_{600} values every 6 hours.

Fecal microbiota transplantation (FMT)

The mice were treated with antibiotics for 1 week before human and mice fecal transplantation experiments. The donor feces were randomly collected from five GBx patients and healthy controls, respectively, which were mixed with saline solution (1 g/ml) and centrifuged to collect the supernatant. Similarly, mice feces from each group were pooled in sterile PBS (20 mg/mL), soaked and shaken, and then filtered through a 100 μm well mesh. The filtered bacterial solution was mixed with 50% glycerol in equal proportion, and then stored at −80 °C. Each mouse received 200 μL bacterial solution intragastrically twice a week along with AOM/DSS treatment. For human fecal transplantation experiments, gavage of the same dose fecal suspension from healthy controls was used as a control. In the mice fecal transplantation experiments, gavage of the same dose of fecal suspension from Sham +AOM/DSS mice was used as a control.

Single bacteria transplantation and intervention

A total of 1×10^8 CFU single bacteria was mixed with 50% glycerol in equal proportion, and then stored at −80 °C. Each mouse received 200 μL bacterial solution or normal saline (NS) intragastrically twice a week along with AOM/DSS treatment. Gavage of the same dose of NS was used as a control. For intervention experiments, BSH inhibitors riboflavin (MCE, HY-B0456) at the dose of 100 mg/kg or 7β-HSDH inhibitor UDCA (MCE, HY13771) at the dose of 50 mg/kg were orally gavaged twice a week during the model establishment.

Cohousing experiment

Age-matched mice from the same breeder were divided into 2 groups, one of which received cholecystectomy, and the other underwent sham surgery. After a one-week period of recuperation, an equal quantity of sham and GBx mice were housed in the same enclosure (Co-housed). Additionally, an equivalent number of sham and GBx mice that were separately accommodated were utilized as the control (Mono-housed). The mono-housed mice were persistently isolated before and throughout the entire process of AOM/DSS experiments. With regard to the co-housed mice, subsequent to a three-week rest, they persisted in being co-housed and were subjected to AOM/DSS treatment. Specifically, an intraperitoneal injection of 12.5 mg/kg AOM was administered, followed by a one-week treatment with 2% DSS in their drinking water. Subsequently, the mice were allowed to rest for one week before repeating this cycle three times. The mice were sacrificed at 18 weeks after the initial AOM injection.

GUDCA or TUDCA or UDCA supplementation

400 mg/kg freshly prepared GUDCA (Solarbio, IG0840) or TUDCA (MCE, HY19696), dissolved in corn oil, was orally gavaged twice a week during administration with AOM/DSS. In addition, GUDCA was dissolved in culture medium to produce a 100 μM solution for organoid treatment. For mice receiving UDCA treatment, the prepared UDCA at a dose of 50 mg/kg was orally administered via gavage twice a week during the establishment of the AOM/DSS model.

OCA treatment

OCA (Selleck, S7660) was dissolved in corn oil. 10 mg/kg of OCA was administered by gavage twice a week during the AOM/DSS modeling. Moreover, 10 μM OCA was used for organoid experimental treatment.

Gut permeability

Mice were fasted overnight and treated with 0.2 mg/g fluorescein isothiocyanate (FITC)-conjugated dextran (Sigma-Aldrich, 53379). Four hours later, the mice were sacrificed and the concentration of FITC-conjugated dextran in plasma was determined by fluorescence spectrophotometry according to the instructions.

Enzyme-linked immunosorbent assay (ELISA)

The concentration of CEA and CA19-9 in serum was measured by ELISA kit (Lifespan Biosciences Inc, Cat.# LS-F5042, Cat.# LS-F37383) according to the manufacturer's instructions.

TOP/FOP-Flash luciferase reporter assay

To determine luciferase reporter activity, TCF luciferase constructs (0.5 μg), containing the WT (pTOPflash) or mutant (pFOPflash) (Sangon Biotech) TCF-binding sites along with 0.1 μg of pRL-TK Renilla luciferase vector (Promega) were co-transfected into HCT116 cells using Lipofectamine 8000 (Beyotime, C0533). Cells were incubated for 48 h and transfected with either control or FXR siRNA (Sangon Biotech) for 24 h followed by measurement of reporter activity using reagents from the Dual-Luciferase kit (Promega, E1960), according to the manufacturer's instructions.

Cell viability assays

HCT116 cells were seeded into 96-well culture plates and transfected with siRNA as described above. Cells transfected with FXR siRNA were treated with 20 μM of Wnt/β-catenin inhibitor, XAV939 (MCE, HY-15147) for 24 h. Cell viability was measured using the CCK-8 assay (Dojindo, CK04), according to the manufacturer's instructions.

Bile acid composition analysis

The content of bile acids in mice was measured by ultra-high-performance liquid chromatography and a QTRAP 6500 + LC-MS/MS System from SCIEX (PANOMIX, Suzhou, China) according to the manufacturer's instructions. The raw data files generated by UPLC-MS/MS were processed using the Analyst software (V.1.7.3). This was done to perform peak integration, calibration, and quantitation for each metabolite. R (V.3.6) was used for data analysis.

BSH analysis

Mouse fecal microbiota precipitate or the cultured *B. breve* precipitate obtained by centrifugation were added with an appropriate amount of PBS (pH 7.4) and homogenized by vortexing for 1 min. Bacterial cells were lysed in an ice bath at 15-second intervals for 90 seconds using ultrasound treatment. The lysed solution was then centrifuged at 13000 g for 30 min at 4 °C and the supernatant was collected into a new tube. The protein concentration was determined by BCA protein kit (Beyotime, P0010), according to the manufacturer's instructions. The protein was diluted to 2 mg/ml with PBS. The BSH activity was predicted by the generation of d5-UDCA from d5-GUDCA by BSH proteins. The reaction was performed in a 200 μl 3 mM sodium acetate buffer (pH 5.2) containing 0.1 mM d5-GUDCA (Santa Cruz Biotechnology, sc-280757) and 0.1 mg/ml protein. The mixture was incubated at 37 °C for 20 minutes and the sample was placed in dry ice to stop the reaction. 100 μl of methanol was added to the mixture and it was vortexed for 5 min. Then, the samples were centrifuged for 20 min at 20000 g at 4 °C. The mixtures were quantified by d5-UDCA with UPLC-MS/MS to determine the BSH activity.

7β-HSDH activity measurement

Mouse fecal microbiota precipitate or the cultured *R. gnavus* precipitate was obtained as described above. The precipitate (0.2 g of wet cells) was then resuspended in 1 ml of extraction buffer containing 0.1 M Tris, 1 mM DTT, 3 mM EDTA, and 10% (v/v) glycerol. After ultrasonic treatment, the bacterial suspension was broken, and the supernatant was collected as a crude enzyme solution. To determine the activity of 7β-HSDH, a total volume of 3 mL of enzyme assay mixture containing 0.5 mM each of GCDCA, GUDCA, and TUDCA, 0.2 mM NADP + , and 10 µl of enzyme solution was used. The reaction mixture without substrate served as a control. The 7β-HSDH activity was expressed as micromoles of NADP+ reduced per minute per milligram of protein, which was determined by the change in NADP(H) concentration (Beyotime, S0179) by monitoring absorbance at 340 nm with a spectrophotometer.

Disease activity index (DAI) assessment and severity of colitis

The severity of colitis was measured using DAI assessment (0-4), a scoring system that includes three parts: body weight loss, rectal bleeding and the stool consistency[46]. We also measured the colon length when the mice were sacrificed to indicate the severity of colitis.

Histopathology and immunohistochemistry staining

The colon and small intestine tissues were dissected along the mesentery, cleaned of fecal contents and rolled into a Swiss-Roll shape from distal to proximal, then stored in 10% neutral-buffered formalin solution for 24 h. The fixed colon tissues were paraffin-embedded and then cut into 5-µm-thick sections and stained with haematoxylin and eosin (H&E) for histologically analysis. The histologic injury scores (0-12) were evaluated in a blinded manner by a gastrointestinal pathologist based on the degree of epithelial damage and inflammatory infiltrate in the mucosa, submucosa and muscularis/serosa[47]. Intestinal tumors were assessed by an experienced pathologist, according to the pathology of mouse models of intestinal cancer: consensus report and recommendations[48,49]. The review mainly focused on the diameter and number of dysplasia/neoplasia/tumors, the depth of tumor invasion, and the area affected by inflammation. Lesions of low (LGD) and high-grade dysplasia (HGD) and adenocarcinoma were graded and counted on each section. In addition, paraffin-embedded and formalin-fixed mouse and human colon tissues samples were used for immunohistochemistry staining, and antibodies used in this procedure including FXR, β-catenin, and c-Myc. Images were taken by NIS-Elements 3.2 (Nikon, Tokyo, Japan).

Quantitative RT-PCR analysis

Mouse colon cancerous tissues were frozen with liquid nitrogen and preserved at −80 °C. The phenol-chloroform extraction was used to extract total RNA. Trizol reagent (Takara, 9109, Japan) and PrimeScript RT reagent Kit (Takara, RR047A, Japan) were chosen in the whole process of RNA extraction, DNA removal and reverse transcription. GAPDH was used as an internal control for RT-PCR. Fecal bacterial total DNA was extracted with a TIANamp STOOL DNA kit (Tiangen, DP328, China) following the supplier's procedure. The 16S rRNA genes of *B. breve* and *R. gnavus* were amplified with universal primers for all bacteria. The RT-PCR primer sequences for colon tissues are summarized in Supplementary Table 2. Primers used to quantify bacteria by qPCR are summarized in Supplementary Table 3.

Nuclear extracts preparation and co-immunoprecipitation (Co-IP)

The nucleus extracts of mice's intestinal cancerous tissues were separated using a nuclear and cytoplasmic fractionation kit (Thermo Scientific, 78833), following the manufacturer's protocol. The nuclear fractions were subjected to co-immunoprecipitation (Co-IP) assay. The Co-IP analysis was performed using Thermo Scientific Pierce co-IP kit (Cat.# 26149). The resulting samples were then analyzed by Western blot to identify binding proteins. Briefly, the nuclear proteins were immunoprecipitated with the prepared protein lysate and corresponding antibody at 4 °C overnight. Protein A/G beads were used to capture the immunoprecipitate and washed 3-4 times with 1 ml lysis buffer after centrifugation at 4 °C, followed by heat elution in 2× loading buffer.

Western blot analysis

The protein extracts derived from mouse colon cancerous and non-tumor tissues were separated using SDS-PAGE electrophoresis and thereafter transferred to a PVDF membrane. The membrane was incubated with specific antibodies to the target proteins overnight at 4 °C, including FXR, β-catenin, c-Myc, TCF4, and GAPDH. Uncropped scans of the blots can be found at the online Source Data.

Isolation and generation of mouse intestinal organoid

Intestines from GBx+AOM/DSS group were washed more than 3 times in ice-cold DPBS (no Mg^{2+}/Ca^{2+}), containing 1% antibiotic-antimycotic (GIBCO, Cat.# 15240-062). Dice the intestines into small pieces (2-4 mm long) to expose crypts and villi. Crypt cells (PBS with 2 mM EDTA) were then isolated using repeated blow washing and a prefabricated crypt isolation solution. Isolated crypts were filtered through a 70 µm nylon cell filter (Falcon, Cat.# 352350) and then counted, dispersed in Matrigel at a density of 200 to 500 crypts/50 µL. Isolated crypts were then cultured in Intesticult organoid growth medium (Stem cell technologies, Cat.# 6005).

Statistics and reproducibility

No statistical method was used to predetermine sample size. Sample sizes were determined based on prior studies in the field and were adequate to detect statistically significant differences between experimental groups. No data were excluded from the analyses. For animal experiments, the mice were randomly assigned before any initial treatments were administered. For in vitro experiments, randomization was unnecessary as the treated cells were derived from the same batch. Additionally, investigators were not blinded to allocations during experiments or outcome assessment.

IBM SPSS Statistics 23 program (IBM SPSS, Turkey) was used for patient statistical analysis. Chi-square test was used to analyze the comparable variables. Graphpad Prism 9.0 software (GraphPad Software Inc., San Diego, USA) was used for experimental statistical analysis. Firstly, we tested whether the data met the conditions of normality and homogeneity of variance. If so, parameter test was selected. If not, the non-parametric test method should be selected. Notably, in the parametric test, we used a two-tailed *t* test for comparison between the two groups. And if multiple groups are compared, ANOVA was used for single-factor multi-group comparative analysis. The following analytical methods were used in this study but were not limited to: Mann-Whitney *U* test, Unpaired *t* test, Welch's *t* test, and ANOVA. Correlation analysis was performed using Pearson correlation analysis. All tests were two-sided unless otherwise specified. Experimental data were shown as mean ± SEM. All data were representative of more than three independent experiments.

Reporting summary

Further information on research design is available in the Nature Portfolio Reporting Summary linked to this article.

Data availability

The raw metagenomic, metabolomic, and RNA-seq sequencing data generated in this study have been deposited in the China National Center for Bioinformation under the accession numbers PRJCA019844, PRJCA040933, and PRJCA040934 and can be accessed using the link (https://ngdc.cncb.ac.cn/bioproject/). The remaining data supporting the findings of this study are provided in the Supplementary information and Source data file. Source data are provided with this paper.

References

1. Unalp-Arida, A. & Ruhl, C. E. Increasing gallstone disease prevalence and associations with gallbladder and biliary tract mortality in the US. *Hepatology* **77**, 1882–1895 (2023).
2. Ahmad, D. S. & Faulx, A. Management of postcholecystectomy biliary complications: a narrative review. *Am. J. Gastroenterol.* **115**, 1191–1198 (2020).
3. Konyn, P. et al. Gallstone disease and its association with non-alcoholic fatty liver disease, all-cause and cause-specific mortality. *Clin. Gastroenterol. Hepatol.* **21**, 940–948.e2 (2023).
4. Di Ciaula, A., Garruti, G., Wang, D. Q. & Portincasa, P. Cholecystectomy and risk of metabolic syndrome. *Eur. J. Intern. Med.* **53**, 3–11 (2018).
5. Schernhammer, E. S. et al. Cholecystectomy and the risk for developing colorectal cancer and distal colorectal adenomas. *Br. J. Cancer* **88**, 79–83 (2003).
6. Zhang, Y. et al. Cholecystectomy can increase the risk of colorectal cancer: A meta-analysis of 10 cohort studies. *PLoS One* **12**, e0181852 (2017).
7. Jiang, X. et al. Cholecystectomy promotes the development of colorectal cancer by the alternation of bile acid metabolism and the gut microbiota. *Front. Med. (Lausanne)* **9**, 1000563 (2022).
8. Xu, Y. et al. Gut microbiota alteration after cholecystectomy contributes to post-cholecystectomy diarrhea via bile acids stimulating colonic serotonin. *Gut Microbes* **15**, 2168101 (2023).
9. Jia, W., Xie, G. & Jia, W. Bile acid-microbiota crosstalk in gastrointestinal inflammation and carcinogenesis. *Nat. Rev. Gastroenterol. Hepatol.* **15**, 111–128 (2018).
10. Wahlström, A., Sayin, S. I., Marschall, H. U. & Bäckhed, F. Intestinal Crosstalk between Bile Acids and Microbiota and Its Impact on Host Metabolism. *Cell Metab.* **24**, 41–50 (2016).
11. Schneider, K. M. et al. Gut microbiota depletion exacerbates cholestatic liver injury via loss of FXR signalling. *Nat. Metab.* **3**, 1228–1241 (2021).
12. Fu, T. et al. FXR regulates intestinal cancer stem cell proliferation. *Cell* **176**, 1098–1112.e18 (2019).
13. Sun, L. et al. Gut microbiota and intestinal FXR mediate the clinical benefits of metformin. *Nat. Med.* **24**, 1919–1929 (2018).
14. Tanaka, M. et al. The association between gut microbiota development and maturation of intestinal bile acid metabolism in the first 3 y of healthy Japanese infants. *Gut Microbes* **11**, 205–216 (2020).
15. Lee, J. Y. et al. Contribution of the 7β-hydroxysteroid dehydrogenase from Ruminococcus gnavus N53 to ursodeoxycholic acid formation in the human colon. *J. Lipid Res.* **54**, 3062–3069 (2013).
16. Yu, J. et al. Farnesoid X receptor antagonizes Wnt/β-catenin signaling in colorectal tumorigenesis. *Cell Death Dis.* **11**, 640 (2020).
17. Almeida, A. et al. A new genomic blueprint of the human gut microbiota. *Nature* **568**, 499–504 (2019).
18. Song, M., Chan, A. T. & Sun, J. Influence of the Gut Microbiome, Diet, and Environment on Risk of Colorectal Cancer. *Gastroenterology* **158**, 322–340 (2020).
19. Housset, C., Chrétien, Y., Debray, D. & Chignard, N. Functions of the Gallbladder. *Compr. Physiol.* **6**, 1549–1577 (2016).
20. Cortés, V. et al. Metabolic effects of cholecystectomy: gallbladder ablation increases basal metabolic rate through G-protein coupled bile acid receptor Gpbar1-dependent mechanisms in mice. *PLoS One* **10**, e0118478 (2015).
21. Roda, E. et al. Enterohepatic circulation of bile acids after cholecystectomy. *Gut* **19**, 640–649 (1978).
22. Pomare, E. W. & Heaton, K. W. The effect of cholecystectomy on bile salt metabolism. *Gut* **14**, 753–762 (1973).
23. Xu, Y. et al. Disordered gut microbiota correlates with altered fecal bile acid metabolism and post-cholecystectomy diarrhea. *Front. Microbiol.* **13**, 800604 (2022).
24. Noh, C. K., Jung, W., Yang, M. J., Kim, W. H. & Hwang, J. C. Alteration of the fecal microbiome in patients with cholecystectomy: potential relationship with postcholecystectomy diarrhea - before and after study. *Int. J. Surg.* **109**, 2585–2597 (2023).
25. Berr, F., Stellaard, F., Pratschke, E. & Paumgartner, G. Effects of cholecystectomy on the kinetics of primary and secondary bile acids. *J. Clin. Invest.* **83**, 1541–1550 (1989).
26. Kullak-Ublick, G. A., Paumgartner, G. & Berr, F. Long-term effects of cholecystectomy on bile acid metabolism. *Hepatology* **21**, 41–45 (1995).
27. Huang, F. et al. Theabrownin from Pu-erh tea attenuates hypercholesterolemia via modulation of gut microbiota and bile acid metabolism. *Nat. Commun.* **10**, 4971 (2019).
28. Gonzalez, F. J., Jiang, C. & Patterson, A. D. An intestinal microbiota-farnesoid x receptor axis modulates metabolic disease. *Gastroenterology* **151**, 845–859 (2016).
29. Wang, Y. et al. Microbial and metabolic features associated with outcome of infliximab therapy in pediatric Crohn's disease. *Gut Microbes* **13**, 1–18 (2021).
30. Guan, B. et al. Bile acid coordinates microbiota homeostasis and systemic immunometabolism in cardiometabolic diseases. *Acta Pharm. Sin. B.* **12**, 2129–2149 (2022).
31. Ward, J. B. J. et al. Ursodeoxycholic acid and lithocholic acid exert anti-inflammatory actions in the colon. *Am. J. Physiol. Gastrointest. Liver Physiol.* **312**, G550–G558 (2017).
32. Ovadia, C. et al. Ursodeoxycholic acid enriches intestinal bile salt hydrolase-expressing Bacteroidetes in cholestatic pregnancy. *Sci. Rep.* **10**, 3895 (2020).
33. Kuang, J. et al. Hyodeoxycholic acid alleviates non-alcoholic fatty liver disease through modulating the gut-liver axis. *Cell Metab.* **35**, 1752–1766.e8 (2023).
34. Nie, Q. et al. Gut symbionts alleviate MASH through a secondary bile acid biosynthetic pathway. *Cell* **187**, 2717–2734.e33 (2024).
35. Quinn, R. A. et al. Global chemical effects of the microbiome include new bile-acid conjugations. *Nature* **579**, 123–129 (2020).
36. Guo, S. et al. Downregulation of the farnesoid X receptor promotes colorectal tumorigenesis by facilitating enterotoxigenic Bacteroides fragilis colonization. *Pharmacol. Res.* **177**, 106101 (2022).
37. Chen, B. et al. Glycoursodeoxycholic acid regulates bile acids level and alters gut microbiota and glycolipid metabolism to attenuate diabetes. *Gut Microbes* **15**, 2192155 (2023).
38. Wu, Q. et al. Suppressing the intestinal farnesoid X receptor/sphingomyelin phosphodiesterase 3 axis decreases atherosclerosis. *J. Clin. Invest.* **131**, e142865 (2021).
39. Zhao, L. et al. A Clostridia-rich microbiota enhances bile acid excretion in diarrhea-predominant irritable bowel syndrome. *J. Clin. Invest.* **130**, 438–450 (2020).
40. Xu, P. et al. Sulfation of chondroitin and bile acids converges to antagonize Wnt/ β-catenin signaling and inhibit APC deficiency-induced gut tumorigenesis. *Acta Pharm. Sin. B.* **14**, 1241–1256 (2024).
41. Wei, D. et al. Melatonin relieves hepatic lipid dysmetabolism caused by aging via modifying the secondary bile acid pattern of gut microbes. *Cell Mol. Life Sci.* **79**, 527 (2022).
42. Sun, D. Q. et al. Farnesoid X receptor activation protects against renal fibrosis via modulation of β-catenin signaling. *Mol. Metab.* **79**, 101841 (2024).
43. Jiang, L., Zhang, H., Xiao, D., Wei, H. & Chen, Y. Farnesoid X receptor (FXR): Structures and ligands. *Comput. Struct. Biotechnol. J.* **19**, 2148–2159 (2021).
44. Ijssennagger, N. et al. Gene expression profiling in human precision cut liver slices in response to the FXR agonist obeticholic acid. *J. Hepatol.* **64**, 1158–1166 (2016).
45. Xiong, X. et al. Obeticholic acid protects mice against lipopolysaccharide-induced liver injury and inflammation. *Biomed. Pharmacother.* **96**, 1292–1298 (2017).

46. Kihara, N. et al. Vanilloid receptor-1 containing primary sensory neurones mediate dextran sulphate sodium induced colitis in rats. *Gut*. **52**, 713–719 (2003).
47. Katakura, K. et al. Toll-like receptor 9-induced type I IFN protects mice from experimental colitis. *J. Clin. Invest*. **115**, 695–702 (2005).
48. Boivin, G. P. et al. Pathology of mouse models of intestinal cancer: consensus report and recommendations. *Gastroenterology*. **134**, 762–777 (2003).
49. Washington, M. K. et al. Patholgoy of rodent models of intestinal cancer: progress report and recommendations. *Gastroenterology*. **144**, 705–717 (2013).

Acknowledgements

The authors wish to thank the specialized statistician Prof. Hui Lin (Department of Epidemiology, Army Medical University, Chongqing, China) for reviewing the statistical analysis. This work was supported by the National Natural Science Foundation of China (Grant No. 82172958 to B.T.) and the Key Program of National Natural Science Foundation of China (Grant No. 82030020 to S.Y.).

Author contributions

B.T., M.Y., and S.Y. designed and supervised the study. B.T., M.Y., S.L., and X.L. performed experiments and analyzed the results. J. H., A.Z., L.W., X.X., and X.L. analyzed the genomic data and performed BA analyses. Y.L., C.L., and J.Z. enrolled patients and collected the patient samples and data. D.T., S.W., J.J., H.J., Z.H., and Y.G. performed laboratory detection. B.T. and M.Y. wrote the original manuscript. C.L., M.Y., and S.Y. reviewed and edited the manuscript.

Competing interests

The authors declare no competing interests.

Additional information

Supplementary information The online version contains supplementary material available at https://doi.org/10.1038/s41467-025-62956-8.

Correspondence and requests for materials should be addressed to Cheng Lu, Min Yang or Shiming Yang.

Peer review information *Nature Communications* thanks Chantal Housset, Hector Palmer and the other, anonymous, reviewer(s) for their contribution to the peer review of this work. A peer review file is available.